

# Numerical Simulation of Proppant Transport in Hydraulic Fractures

Morteza Roostaei, Alireza Nouri, Vahidoddin Fattahpour, Dave Chan

Department of Civil and Environmental Engineering, University of Alberta

## Abstract

A central issue in hydraulic fracturing treatment in petroleum wells is the transport of proppant particles by the injection fluid. In this paper, we present an innovative proppant transport model in a fixed rectangular- and elliptic-shaped slots. The proposed model is an improvement to the current modeling of proppant transport by applying a non-oscillatory numerical scheme which has high accuracy everywhere in solution domain, even close to the steep gradients. In addition, inertia, fracture wall, and concentration effects on proppant settling along with slurry evolution as a function of proppant concentration has been considered.

This paper introduces the mathematical equations that govern the proppant transport phenomenon and discusses special front capturing numerical techniques, boundary conditions, coupling between proppant and slurry mass conservation equations and time stepping restrictions required for the solution stability. We incorporated published correlations obtained from proppant transport laboratory experiments in our numerical model to better capture the physics of the problem. 5<sup>th</sup>-order WENO scheme was used to avoid oscillation and diffusion at the proppant front since traditional finite difference discretization was found to be insufficient in solving the hyperbolic transport partial differential equations. Results show that the technique used in this study can capture the proppant distribution with minimum oscillation and diffusion.

A series of sensitivity analysis was conducted to explore the legitimacy of these assumptions and to provide guidelines that allow more accurate predictions of the proppant and fluid transfer. Numerical results are presented to show how proppant distribution is impacted by the injection fluid viscosity, density difference between proppant particles and injection fluid, proppant size, and fluid flow injection rate. Results of the sensitivity analysis illustrate the significance of choosing appropriate viscosity of the injection fluid as small changes in the viscosity may cause noticeable effects on the concentration distribution. In addition, we found that variation of proppant size and density within a reasonable range have a modest effect on proppant concentration distribution.

Furthermore, we also investigated the amount of gravity driven vertical motion of proppant which is driven by density differences (convection) and compare it to a second gravity driven motion which is proppant settlement. Both of these two well recognized mechanisms can occur inside a fracture during proppant placement, however, the importance of each mechanism as a function of proppant injection design parameters is not fully understood.

**Keywords:** Frac-Packing, Hydraulic Fracturing, Proppant Transport, Shock Capturing Techniques

## 1. Introduction

In the earliest type of proppant transport model, after discretizing the fracture into vertical sections, leak off, concentration increase and proppant's settling velocity are calculated for each section (Daneshy, 1978; Novotny, 1977). Based thereupon in the next step, the amounts of deposited and suspended sand concentrations are computed. The final bed shape can also be obtained after the injection has stopped. These models need a settling velocity correlation for proppant in relation to such parameters as the proppant and injection fluid properties. Novotny (1977) incorporated heat transfer between proppant slurry and the formation in this type of modeling. The model is limited to planar vertical fractures and important physical issues of the transport problem, such as two-dimensional flow inside the fracture, cannot be captured.

Another more general proppant transport modelling category was later introduced that solves the partial differential equations (PDEs) for conservation of mass of proppant and slurry and is very flexible in the sense that additional physics can be easily incorporated in the simulation (Lavrov, 2011). As an example of such physics, the fluid and proppant velocity fields have originally been assumed to be the same. In other words, it was assumed that no slippage happens between the fluid and the proppant and thus no momentum transfers between the carrying fluid and the proppants. Later, laboratory experiments showed that proppant and fluid velocities are different in both horizontal and vertical directions (Liu, 2006). Empirical correlations have been included in the numerical model to account for this effect (Friehauf, 2009).

Most often, no diffusion of proppant particles is assumed to occur in proppant transport in hydraulic fractures. Thus, the front of the proppant concentration profile remains sharp (Adachi et al., 2007). In addition, both proppants and injection fluid are assumed to be incompressible. Typically, the lubrication theory approximation (Reynolds equation) is used to describe the relationship between slurry velocity and pressure gradient. An essential element of this theory is averaging of the field variables, such as the solids volume fraction and the fluid velocity, in the direction perpendicular to the fracture walls. For the lubrication theory to be a valid approximation, a collection of criteria for development lengths must be satisfied. The discussion of these conditions is outside the scope of this work and more details can be found elsewhere (Pearson, 1994).

Many modifications have been made in the original models by different researchers to better simulate the transport phenomena. Settari et al. (1990) was the first to propose the concept of partially decoupled fracture modeling. In his approach, he linked a fracture simulator to a fluid flow simulator and mapped the fracture geometry in terms of permeability and porosity onto the reservoir simulator grids. Later, several researchers used this approach in their numerical simulation of proppant transport. Miranda et al. (2010), Shaoul et al. (2007), and Behr et al. (2006) linked a commercial reservoir simulator to a commercial fracture and proppant simulator and used the same concept that Settari et al. (1990) had used for frac-pack analysis. Later, other methods have been proposed for numerical simulations of proppant transport (Friehauf, 2009; Liu, 2006;

Sharma & Gadde, 2005; Gadde et al., 2004; Ouyang, 1994). These new class of simulations can be categorized as fully decoupled models in which only the fracture and proppant distribution are simulated, without paying attention to the reservoir simulations. Ouyang (1994) proposed an adaptive re-meshing technique for the hydraulic fracture simulation that was adopted in a later work by Rebeiro (2013) for proppant injection simulations. Friehauf (2009), Liu (2006), and Gadde et al. (2004) used PKN fracture geometry and included some of the experimental works in the literature related to proppant transport in their numerical model.

Adachi (2007) in his proppant transport modeling assumed the incompressibility of the proppant and the slurry, which is an acceptable assumption for liquid fracturing fluids. Further, he assumed that the only mechanism to account for “slip” between the proppant and the carrying fluid is gravity-induced settling. This implies that, in the absence of gravity, the proppant and fluid move at the same velocity. He did not present the type of settling equation, if any, that was used. In addition, in his fracture simulator he employed an analytical integral equation between slot width and pressure.

Another important piece of work has been published by Barrie and Conway (1994; 1995), which served as a validation to the commercial proppant simulator GOHFER. The basic theory of GOHFER is based on the corrected Stokes equation to consider the effect of proppant concentration through an empirical equation of Govier and Aziz (1972). Barrie and Conway fracture simulator again uses an integral equation between fracture width and pressure (integral of the displacement for the point load over the surface of the fracture) (Al-quraishi et al., 1999; Bayo Shokir et al., 2007).

Mobbs et al. (2001), Unwin et al. (1995), and Hammond (1995) published their simulations with the objective of investigating the effect of flow profile on final proppant distribution. They considered homogeneous flow (in which proppant particles are uniformly distributed across the fracture width) and sheet flow (in which some unspecified, but rapid, process has caused all proppant to migrate across the fracture width into a close-packed sheet at the fracture center). They assumed constant and elliptical PKN fracture width. They also neglected retardation and did not modify Stokes law. They concluded that both settling and convection can occur during the treatment and cannot be neglected.

Probably, the most complete works in proppant transport simulation are the ones published by Friehauf (2009), and Gadde (2004). Friehauf (2009) and Gadde (2004) incorporated the experimental correlations of proppant retardation and settlement obtained by Liu (2006) in a numerical code. The main deficiency of these models is the use of conventional finite difference schemes in solving the transport PDEs.

Another class of modeling of particle transport is based on the concepts of granular kinetic theory proposed by Eskin and Miller (2008). They considered steady-state flow of slurry which can be considered a significant limitation of the model as extending it to transient flows may make it computationally prohibitive for any practical use in a coupled hydraulic fracturing simulation. Many of the equations in their model use empirical laws and correlations and are therefore valid

only within certain ranges. Leak-off was neglected in the numerical computations (its introduction should be straightforward, if needed, though).

In all published numerical models, the transport and placement of proppant within the fracture is usually modeled by representing the slurry as a two-component, interpenetrating continuum. This implies that the fluid flow equations (i.e., conservation of mass and conservation of momentum) are solved for the slurry, and not for each individual component. In this paper, we follow the same procedure and solve the mass balance equation of the proppant and slurry. However, we improve the current proppant modeling by capturing more phenomena including correct settlement of particles and differential velocity between fluid and particles. Further, we remove numerical diffusion, by applying a more accurate numerical technique specially designed for advection phenomena.

## **2. Mathematical Formulation and Solution Technique**

The governing equations of a proppant transport model are: a) conservation of mass for the injection fluid, which yields the pressure distribution, b) conservation of mass for the solid proppants which yields the proppant concentration distribution during the simulation, c) momentum equations which for the case of flow between parallel plates leads to the cubic law that is a relation between pressure gradient and fluid velocity, and d) proppant settling velocity or the terminal velocity of the proppant particles inside the fracture. The main output of this kind of modelling is the distribution of the proppant that is given by its volumetric concentration (defined as the volume of the proppant over the volume of the slurry).

In our simulations, we have neglected flocculation and slumping of the particles and we assumed uniform concentration across the width of the fracture (slot). The latter assumption avoids unnecessary complications arising from large aspect ratio of elements in the numerical model or high running time of a model with large number of elements. Therefore, a 2D modeling of the problem seems sufficient.

In addition, for the binary system of proppant flow, Taylor dispersion, which consists of diffusion associated with the molecular movement, turbulent flow and temperature gradient (Bird et al., 1976) can be neglected. The most obvious consequence of these assumptions is that this moving boundary problem consists of a sharp proppant front (without any diffusion ahead) which needs special numerical techniques.

The Finite Volume Method (FVM) technique which utilized to minimize numerical dispersion that occurs in traditional Finite Difference (FD) schemes. A 5<sup>th</sup> order WENO scheme was adopted which unlike traditional FD schemes or flux limiters methods, gives non-oscillatory, high order accuracy solution both anywhere the solution is smooth (away from proppant front) and near discontinuities (proppant front).

### **2.1 Mass Balance Equations**

Conservation of mass equations for slurry flowing through a constant width slot and the proppant that it carries down the slot assuming incompressible fluid and proppant are:

For injection fluid:

$$\frac{\partial w}{\partial t} + \frac{\partial}{\partial x}(u_{sl}w) + \frac{\partial}{\partial y}(v_{sl}w) + q_{inj} = 0 \quad (1)$$

For proppant:

$$\frac{\partial}{\partial t}(cw) + \frac{\partial}{\partial x}(u_p cw) + \frac{\partial}{\partial y}(v_p cw) + cq_{inj} = 0 \quad (2)$$

$$u_{sl} = cu_p + (1 - c)u_f \quad (3)$$

$$v_{sl} = cv_p + (1 - c)v_f \quad (4)$$

where  $c$  is the volumetric proppant concentration defined as the ratio of proppant volume to slurry volume,  $u_p$  and  $u_f$  are horizontal velocities of proppant and fluid and  $v_p$  and  $v_f$  are vertical velocities of proppant and fluid.

Fluid velocity inside a hydraulic fracture for Newtonian fluids is related to the pressure gradient ( $\frac{\partial p}{\partial x}$ ) inside the fracture. Momentum conservation equation or Navier-Stokes equation describes the motion of a fluid as a relationship between flow velocity (or momentum) and pressure. In hydraulic fracturing applications, the solution to the Navier-Stokes equation is called cubic law (Economides & Nolte, 2000):

$$u_{sl} = -\frac{w^2}{12\mu_{sl}} \frac{\partial p}{\partial x} \quad (5)$$

Similarly, for  $y$  direction:

$$v_{sl} = -\frac{w^2}{12\mu_{sl}} \frac{\partial(p - \rho_{sl}gy)}{\partial y} \quad (6)$$

where  $u_{sl}$  and  $\rho_{sl}$  are the equivalent viscosity and density of the slurry, respectively. By applying cubic law, which indeed relates pressure gradient to the velocity field, the number of unknowns ( $c$ ,  $p$ , velocity) becomes the same as the number of equations. If we substitute Eq. (5) and (6) in Eq. (1), we obtain:

$$\frac{\partial}{\partial x} \left( \frac{w^3}{12\mu_{sl}} \frac{\partial p}{\partial x} \right) + \frac{\partial}{\partial y} \left( \frac{w^3}{12\mu_{sl}} \frac{\partial(p - \rho_{sl}gy)}{\partial y} \right) + q_{inj} = \frac{\partial w}{\partial t} \quad (7)$$

The right-hand side of the equation disappears for the case of flow through fixed slots since the width is constant. We adopted traditional central finite difference scheme to solve this elliptic PDE and obtain the fluid pressures.

The rheology of the slurry is affected by the proppant concentration. We assumed the increase in viscosity can be described by the following expression (Barree & Conway, 1994):

$$\mu = \frac{\mu_0}{\left(1 - \frac{c}{c^*}\right)^{1.82}} \quad (8)$$

where  $c^*$  is the saturation concentration and  $\mu_0$  is the initial viscosity of the clean fluid. Saturation concentration corresponds to the maximum concentration that can be achieved by random packing of regular spheres. At saturation concentration, proppant particles create a pack and behave like solid porous medium. Thereafter, only the fluid phase can mobilize through the pack. Saturation concentration can be determined experimentally and depends on the type of the proppant and it varies between 0.52 (loose packing) and 0.65 (dense packing) (for example see Horri et al., 2011; Koos et al., 2012). We assigned a value of 0.6 to this parameter in the simulations.

### 3. Numerical Solution Technique

The complexity of the proppant transport problem comes from solving the hyperbolic PDE of proppant transport (Eq. 2). The solution to hyperbolic PDEs is highly dependent on the specified initial conditions. Solution to hyperbolic PDEs simply transports the initial condition within the model. On the other hand, it is well known that hyperbolic partial differential equations (PDE) accept both smooth as well as discontinuous solutions. A discontinuous solution, also referred to as a shock, is characterized by large gradients in the variables such as concentration. Accurate numerical simulation of such systems is a challenging task using conventional numerical methods. The numerical challenge in the vicinity of large gradients (shocks) is that high order FD schemes lead to significant oscillations despite the fact that such schemes result in higher accuracy in smooth regions. On the other hand, first-order methods provide non-oscillatory (monotonic) solution near the shocks, while giving poorer accuracy in the smooth regions (Leveque, 2004).

The first proposed successful idea in obtaining a uniformly high order accurate, yet non-oscillatory results was proposed by Harten et al. (1987). The method was named ENO which stands for essentially non-Oscillatory. These researchers used Newton divided differences to measure the local smoothness of the stencils. Later, WENO schemes (Weighted ENO) were developed based on ENO schemes to reduce the computational cost and increase the accuracy order (Liu et al., 1994, Jiang and Shu, 1996).

To avoid complications arising from un-split WENO schemes, we utilized dimensional splitting method, a type of fractional step method, to solve Eq. 2. Using this method, a multi-dimensional PDE with source terms can be split into several 1-dimensional PDEs (depending on the dimensionality of the problem) and an ordinary differential equation. In our case, Eq. 2 becomes:

$$\frac{\partial(c)}{\partial t} + cq_{inj} = 0 \quad (9)$$

$$\frac{\partial c}{\partial t} + \frac{\partial[u_p(x, y)c(x, y)]}{\partial x} = 0 \quad (10)$$

$$\frac{\partial c}{\partial t} + \frac{\partial[v_p(x, y)c(x, y)]}{\partial y} = 0 \quad (11)$$

This set of equations is solved by the 5<sup>th</sup> order WENO scheme combined with the 4<sup>th</sup> order Runge-Kutta method. To better explain WENO scheme, we consider Eq. 10 and write it in the following form:

$$\frac{\partial c}{\partial t} + \frac{\partial f}{\partial x} = 0 \quad (12)$$

where:

$$f = u_p(x, y)c(x, y) \quad (13)$$

Integrating Eq. 12 over the grid cell obtains:

$$\frac{dC(x_i, t)}{dt} = -\frac{1}{\Delta x_i} [f(x_{i+\frac{1}{2}}, t) - f(x_{i-\frac{1}{2}}, t)] \quad (14)$$

where the average value of proppant concentration over a grid block  $i$  at time  $t_n$  can be expressed as:

$$C_i^n \approx \frac{1}{\Delta x_i} \int_{x_{i-\frac{1}{2}}}^{x_{i+\frac{1}{2}}} c(x, t_n) w(x, t_n) dx \quad (15)$$

We approximate Eq. 14 by the following conservative scheme:

$$\frac{dC(x_i, t)}{dt} = -\frac{1}{\Delta x_i} [\hat{f}_{i+\frac{1}{2}} - \hat{f}_{i-\frac{1}{2}}] \quad (16)$$

The function,  $\hat{f}$  is a monotone numerical flux. There are many examples of such a flux and here we adopted Lax-Friedrichs monotone flux (Leveque, 2004):

$$\hat{f}_{i+\frac{1}{2}} = \frac{1}{2} [f(x_i) + f(x_{i+1}) - \alpha_{i+\frac{1}{2}}(f(x_{i+1}) - f(x_i))] \quad (17)$$

and

$$\alpha_{i+\frac{1}{2}} = \max_{(c_i, c_{i+1})} |f'| \quad (18)$$

Eq. 16 is solved by applying the 4<sup>th</sup> order Runge-Kutta method in which  $C_i^n$  will be obtained by WENO method. WENO starts by finding a polynomial  $p_i(x)$ , of degree at most  $k - 1$ , based on cell averages  $C_i(x)$ , such that it is a  $k^{th}$  order accurate approximation of the unknown function  $c(x)$ :

$$p_i(x) = c(x) + O(\Delta x^k) \quad (19)$$

In other words, the unique polynomial  $p_i(x)$  has the following property:

$$\frac{1}{\Delta x_i} \int_{x_{i-\frac{1}{2}}}^{x_{i+\frac{1}{2}}} p(x, t_n) dx = C_i \quad (20)$$

We use symbol  $S(i)$  to show the stencil based on  $r$  cells to the right and  $s$  cells to the left:

$$S(i) = \{I_{i-r}, \dots, I_{i+s}\} \quad (21)$$

and we know that:

$$r + s = k - 1 \quad (22)$$

It can be shown that the  $k^{th}$  order accurate polynomial that we are looking for can be found by:

$$p_i \left( x_{i+\frac{1}{2}} \right) = c_{i+\frac{1}{2}} = \sum_{j=0}^{k-1} b_{rj} C_{i-r+j} \quad (23)$$

where  $b_{rj}$  are the constant coefficients of the polynomial. Shu (1997) using the Lagrange form of the interpolation polynomial obtained the following expression for non-uniform grids:

$$b_{rj} = \left( \sum_{m=j+1}^k \frac{\sum_{l \neq m}^k \prod_{p=0, p \neq m, l}^k (x_{i+\frac{1}{2}} - x_{i-r+p-\frac{1}{2}})}{\prod_{l=0, l \neq m}^k (x_{i-r+m-\frac{1}{2}} - x_{i-r+l-\frac{1}{2}})} \right) \Delta x_{i-r+j} \quad (24)$$

For a uniform grid, above expression reduces to:

$$b_{rj} = \left( \sum_{m=j+1}^k \frac{\sum_{l \neq m}^k \prod_{p=0, p \neq m, l}^k (r - p + 1)}{\prod_{l=0, l \neq m}^k (m - l)} \right) \quad (25)$$

In solving a hyperbolic PDE, we know that we have the point values of the unknown at the nodes, from initial conditions. In WENO method, these nodal values are used to approximate a high order accurate derivative of the function. In other words, knowing the point values:

$$c_i = c(x_i), \quad i = 1, 2, \dots, N \quad (26)$$

a numerical flux function should be found based on nodal values:

$$\hat{C}_{i+\frac{1}{2}} = \hat{C}(C_{i-r}, C_{i-r+1}, \dots, C_{i+s}), \quad i = 0, 1, 2, \dots, N \quad (27)$$

such that the flux difference approximates the function derivative to the  $k^{th}$  order accuracy:

$$\frac{1}{\Delta x_i} \left( \hat{C}_{i+\frac{1}{2}} - \hat{C}_{i-\frac{1}{2}} \right) = C'(x_i) + O(\Delta x^k), \quad i = 0, 1, 2, \dots, N \quad (28)$$

Again, it can be shown that the coefficients  $c_{rj}$  defined above can be used to achieve such a property:

$$\hat{C}_{i+\frac{1}{2}} = \sum_{j=0}^{k-1} b_{rj} c_{i-r+j} \quad (29)$$

In WENO if, for example,  $2k - 1$  cells are used to give  $k$  stencil candidates, all  $k$  stencil candidates are used to give  $2k - 1$  order accuracy. To be more precise, a convex combination of all the candidate stencils is used. If we show all the stencil candidates by:

$$S_r(i) = \{x_{i-r}, \dots, x_{i-r+k}\}, \quad r = 0, \dots, k - 1 \quad (30)$$

and  $k$  different numerical fluxes by:

$$\hat{C}_{i+\frac{1}{2}}^{(r)} = \sum_{j=0}^{k-1} b_{rj} c_{i-r+j} \quad (31)$$

WENO uses a convex combination of all the candidates as:

$$\hat{C}_{i+\frac{1}{2}} = \sum_{r=0}^{k-1} \omega_r \hat{C}_{i+\frac{1}{2}}^{(r)} \quad (32)$$

For stability and consistency, weights  $\omega_r$  should follow below requirements:

$$\omega_r \geq 0, \quad \sum_{r=0}^{k-1} \omega_r = 1 \quad (33)$$

The way that the weights,  $\omega_r$ , are defined to create the convex combination is different in smooth regions and near discontinuity. In smooth regions the weights are shown by  $d_r$ :

$$\hat{C}_{i+\frac{1}{2}} = \sum_{r=0}^{k-1} d_r \hat{C}_{i+\frac{1}{2}}^{(r)} \quad (34)$$

$d_r$  weights are always positive. When a discontinuity exists in the region, the corresponding weights  $\omega_r$  would be zero. Originally, polynomials or rational functions were used to define weights since they are computationally efficient:

$$\omega_r = \frac{\alpha_r}{\sum_{s=0}^{k-1} \alpha_s}, \quad r = 0, \dots, k-1 \quad (35)$$

with

$$\alpha_r = \frac{d_r}{(\varepsilon + \beta_r)^2} \quad (36)$$

In the above equation  $\varepsilon$  is introduced to avoid denominator from becoming zero. A value of  $\varepsilon = 10^{-6}$  has been suggested for this purpose. In WENO method, the smoothness of each stencil is measured through a parameter  $\beta_r$  which is called smooth indicator. Jiang and Shu, (1996) after extensive experiments, proposed following relationship for smooth indicators:

$$B_r = \sum_{l=1}^{k-1} \int_{x_{i-\frac{1}{2}}}^{x_{i+\frac{1}{2}}} \Delta x^{2l-1} \left( \frac{\partial^l p_r(x)}{\partial x^l} \right)^2 dx \quad (37)$$

#### 4. Convection and Settling of Proppants

Settling and convection are the two controlling mechanisms in proppant placement. Single particle settling velocity in an unbounded medium in Stokes regime (low Reynolds number regime) can be expressed as:

$$v_t = \frac{g d_p^2 (\rho_p - \rho_f)}{18\mu} \quad (38)$$

This terminal velocity has been obtained by neglecting the convective term from the Navier-Stokes equation. In creeping flow regime, since the Reynolds number is very low, no wake is generated

at the back of the particle. In this region, an analytical solution to Navier-Stokes equation for the drag force  $C_D$  on a sphere can be found (Stokes, 1850, Batchelor, 1972) which leads to Eq. 38. At high Reynolds numbers, no analytical solution exists for the flow of fluid past a sphere and experimental results possess more value. Different forms of curve fitting for terminal falling velocities experimental data has been carried out during almost a hundred of years. Based on experimental data of Allen (1900), Wieselsberger (1922), Prandtl and Tietjens (1931), and Schiller (1932), a log-log graph of drag coefficient versus Reynolds number has been well established. This graph is called “standard drag curve” where  $C_D$  is plotted against Reynolds number.

The relationships between Reynolds number and drag coefficient are inconvenient in giving explicit expressions of terminal velocity, since in both of these dimensionless numbers, terminal velocity is involved and an iterative procedure is needed. However, the terminal velocity can be omitted by defining another dimensionless parameter:

$$Ga = \frac{3}{4} C_D Re^2 = \frac{d_p^3 g \rho_f (\rho_p - \rho_f)}{\mu^2} \quad (39)$$

where  $Ga$  is Galileo Number (Clift et al. 1978). It can be seen that Galileo number is independent of terminal velocity and can be evaluated from physical properties of the proppant and carrying fluid. Therefore, for proppant transport simulations, it is more satisfactory to express Galileo number rather than drag coefficient as a function of Reynolds number. We plotted Reynolds number as a function of Galileo number, from data in standard drag curve. The settling velocity of particles is found by calculating Reynolds number and using Fig. 1.

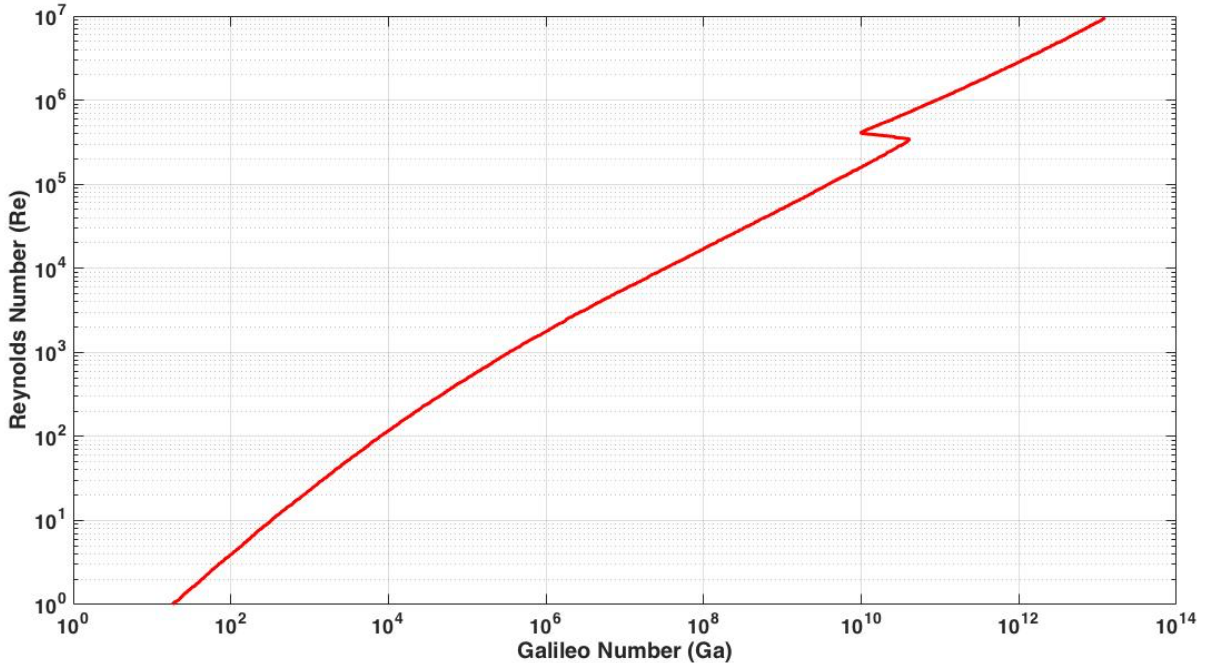


Figure 1: Reynolds Number vs Galileo Number

In addition to inertia, actual settling velocity of proppants inside fracture deviates from single terminal velocity due to the presence of fracture wall and other particles, which in turn modify the flow field. It is well established that when a particle is settling in a liquid, the confining walls around the system produce retardation effect on the particle. In other words, terminal settling velocity of proppants is known to be lower in a confined liquid compared to the case that no walls are present under identical conditions. Moreover, the presence of other particles will change the drag force exerted on each particle. The motion of other particles creates a “return flow” of carrying fluid.

Therefore, terminal velocity should be corrected for the effect of fracture walls and concentration. We assumed that these phenomena have a multiplicative effect on terminal velocity:

$$v_p = v_{inertia} f(w) f(c) \quad (40)$$

where  $v_{inertia}$  is found from Fig. 1 based on Reynolds number,  $f(w)$  is accounts for the wall effects and  $f(c)$  include the concentration effect. Among all the available experimental wall and concentration factors, we selected Miyamura et al. (1981) wall factor and Barree et al. (1994) concentration factor:

$$f(w) = R_0 + \sum_{i=1}^{19} R_i \left( \frac{d_p}{w} \right)^i \quad (41)$$

$$f(c) = e^{-5.9c} \quad (42)$$

where  $R_i$  are experimental coefficients,  $w$  is fracture width and  $c$  is proppant concentration. Therefore, the proppant settling velocity can be written as:

$$v_p = -\frac{w^2}{12\mu_{sl}} \frac{\partial p}{\partial y} + \frac{w^2}{12\mu_{sl}} \frac{\partial(\rho_{sl} g y)}{\partial y} - v_{inertia} \left( R_0 + \sum_{i=1}^{19} R_i \left( \frac{d_p}{w} \right)^i \right) e^{-5.9c} \quad (43)$$

It should be emphasized that the second term in Eq. 43 is convection velocity the topic of which will be discussed later.

Comparing settling and convection velocities (Eq. 38 and second term of Eq. 43), it can be concluded that convection is scaled to fracture width while settling is scaled to proppant diameter. Since proppant entry requirement states that the fracture width should be at least 4 to 5 times larger than the proppant diameter and also convection is related to width to the power of two, while settling is related to proppant diameter to the power of two, it is reasonable to expect that convection has a much larger effect than settling on proppant placement. Convective flow can be quantified and measured based on fluid rheological properties and local proppant concentration. Ratio of the horizontal force to vertical force exerted on unit length of fluid yields a dimensionless group called Buoyancy number which is useful in predicting dominance of horizontal or vertical flow (Clark and Zhu, 1996):

$$N_{Bu} = \frac{12\mu}{\Delta\rho \cdot g \cdot w^3} \cdot \frac{Q_h}{h} \quad (44)$$

Buoyancy number is the ratio of the axial flow velocity to the typical convection velocity, driven by gravity due to density differences. The lower the Buoyancy number, the stronger the convection mechanism. This dimensionless parameter can be seen as an indicator of the relative importance

of convection and horizontal flow. It can be observed from Eq. 44 that  $N_{Bu}$  is extremely sensitive to changes in the width of the fracture.

## 5. Algorithm for Coupling Slurry and Proppant Transport Equations

We designed a coupling algorithm to link the partial differential equations for fluid flow and proppant transport. Two variables are important in our coupling: proppant velocity which is a direct result of solving fluid flow and slurry mass conservation, and slurry viscosity which is adjusted for proppant concentration changes through Eq. 8 (or any of the empirical equations in the literature). Fig. 2 shows the coupling scheme for the slurry and proppant mass balance solvers. According to the figure, the latest pressure distribution from Eq. 7 is used to calculate the proppant velocities needed in solving Eqs. 10 and 11 to obtain the latest concentration. Then the fluid rheological properties are updated as a function of this new concentration. Since the proppant transport PDE is solved explicitly, we imposed a Courant–Friedrichs–Lewy (CFL) stability condition on the time step that assures information travels within one element in each time step.

To provide a numerical solution for the proppant transport partial differential equation, we applied a simple iteration approach. The proppant mass balance partial differential equation that we obtained in the previous section is non-linear, meaning that the coefficients of the equation depend on the unknown. At each time-step the transport problem is divided into three parts:

First, we calculate the coefficients of the slurry mass balance equation (Eq. 7) using viscosity of the previous time step (at time level  $n - 1$ ) or at the previous iteration level,  $k - 1$ . We solve for the pressure field using the viscosity obtained in the previous time-step (or the initial condition for the first time-step); Next, we calculate the vertical and horizontal velocity of the proppant, using the pressure field calculated in the previous time-step (Eqs. 5 and 43). Finally, we apply a finite-volume method to Eqs. 10 and 11 to advect the concentration of proppant.

We iterate on the solution until convergence is achieved. Fig. 2 shows the coupling between the slurry and proppant mass balance solvers.

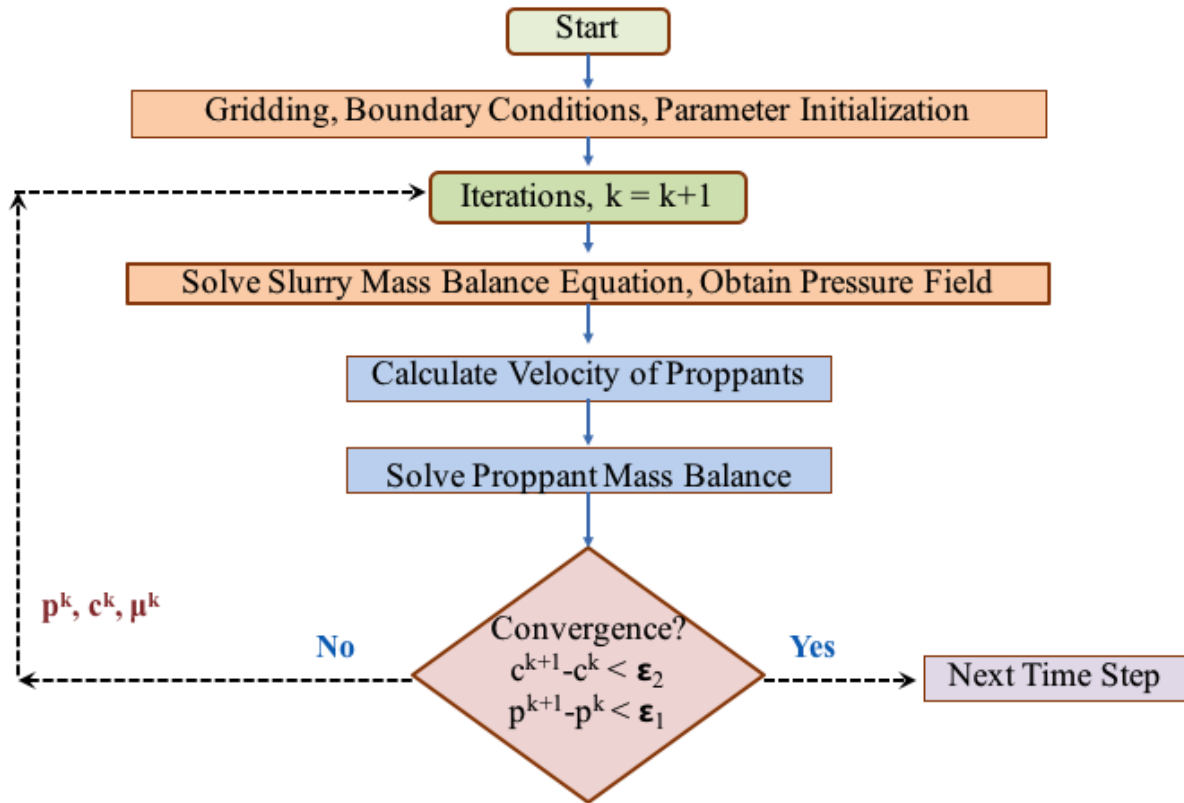


Figure 2: Numerical Algorithm of Solving System of Mass Balance Equations

## 6. Numerical Example

The result of any numerical work should be validated by a comparison with experiments. However, there are some restrictions in the published experimental works that prevent such a comparison. The main issue is that majority of the available experimental works have employed a non-Newtonian injection fluid (Clark, 1996; Bayo Shokir, 2007). One of the main assumptions of our simulation is that the fluid is Newtonian. Now the major issues that arise when comparing such works with our results are:

1. The most important parameter describing proppant movement in fracture is its settling velocity, which is a function of the rheological behavior of the fluid. Non-Newtonian fluids present a series of characteristics including plasticity, yield stress and time-dependent behavior. In contrast to the extensive literature on settling in Newtonian media, much less work has been carried out on the free settling in non-Newtonian fluids. In non-Newtonian fluids, settling velocity change due to inertia, wall effect and proppant concentration follows complex correlations. The viscosity evolution of slurry will also be more complex. All the correlations applied in our code for the effect of fracture walls, inertia and concentration on proppant settling velocity are specifically proposed for Newtonian fluids. Indeed, there is a lack of well-established correlations for other types of fluids.
2. Even if it is assumed that Newtonian fluids' settling velocity correlations and corrections can be applied to non-Newtonian fluids, the results of experimental work gives a general

idea of the shape of the concentration plume at certain times, but they never provide the proppant concentration, or the proppant bank build-up is not very clear in them (As an example see Clark 1996; Barree and Conway, 1994 and 1995; Liu and Sharma, 2005; Liu et al., 2006). This is due to the fact that the exact amount of proppant concentration cannot be measured during the tests.

3. From numerical point of view, the flow of power-law fluids inside fracture follows the general form of cubic law (Friehauf and Sharma, 2008):

$$q_x = -\frac{n}{2n+1} K^{\frac{1}{n}} \frac{w^{\frac{2n+1}{n}}}{2^{\frac{n+1}{n}}} \left[ \left( \frac{dp}{dx} \right)^2 + \left( \frac{dp}{dy} \right)^2 \right]^{\frac{1-n}{2n}} \frac{dp}{dx} \quad (44)$$

In case of Newtonian fluids, since the consistency index (n) is 1, the relationship between flow rate and pressure will be linear and accordingly, a linear system of equation needs to be solved to obtain pressure field. However, such a complex relation between pressure and flow rate in non-Newtonian fluids make the system of equations non-linear and accordingly the running time of the simulation will become significantly longer.

Therefore, we only verified our model by comparing the results of our simulations with commercial software COMSOL Multiphysics.

A synthetic model with realistic parameters was designed for a series of computer simulations to investigate the effects of volumetric proppant injection rate, injection fluid density, proppant size, carrying fluid viscosity, fracture shape and Buoyancy number on proppant settling and convection inside a fixed dimension slot. This section first presents the results of model verification against the results of a commercial PDE solver (COMSOL Multiphysics) for rectangular and elliptic shape fractures with constant fracture length, width and height. We first describe a base case model whose input parameters are used in the sensitivity study simulations except for one parameter which is changed at a time. In all cases the fracture is rectangular with a uniform width of 3 mm.

### 6.1 Geometry and Boundary Conditions

For the verification simulation, the model domain is fixed at 5 m by 5 m with 3-mm uniform slot aperture. Initially the slot is filled with the injection fluid (no proppant). Fig. 3 shows the domain and boundary conditions. The slurry injection was assigned a rate of 1.325 l/s (0.001325 m/s) with 0.3 proppant concentration at the left boundary (inlet) over the full slot height. Top, bottom, and right boundaries were assigned zero proppant flux (solid wall boundary condition) to prevent proppant from exiting the model. Fluid was assigned zero pressure at the right boundary and was not allowed to exit from the top and bottom boundaries.

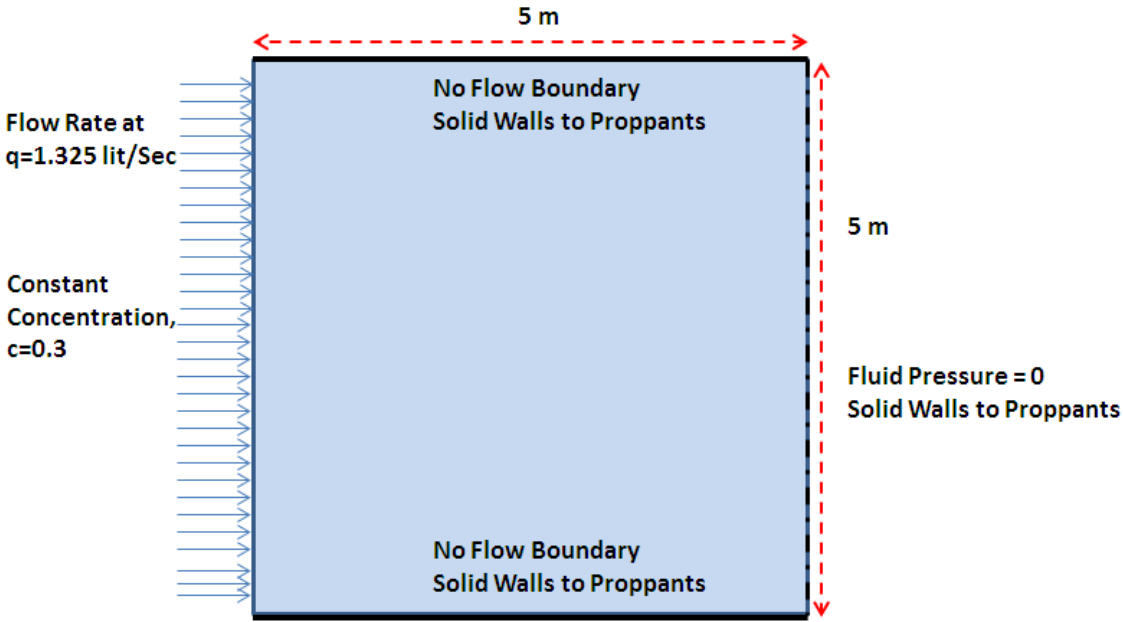


Figure 3: Model domain and boundary conditions for slurry and proppant transport equations

## 6.2 Model Verification

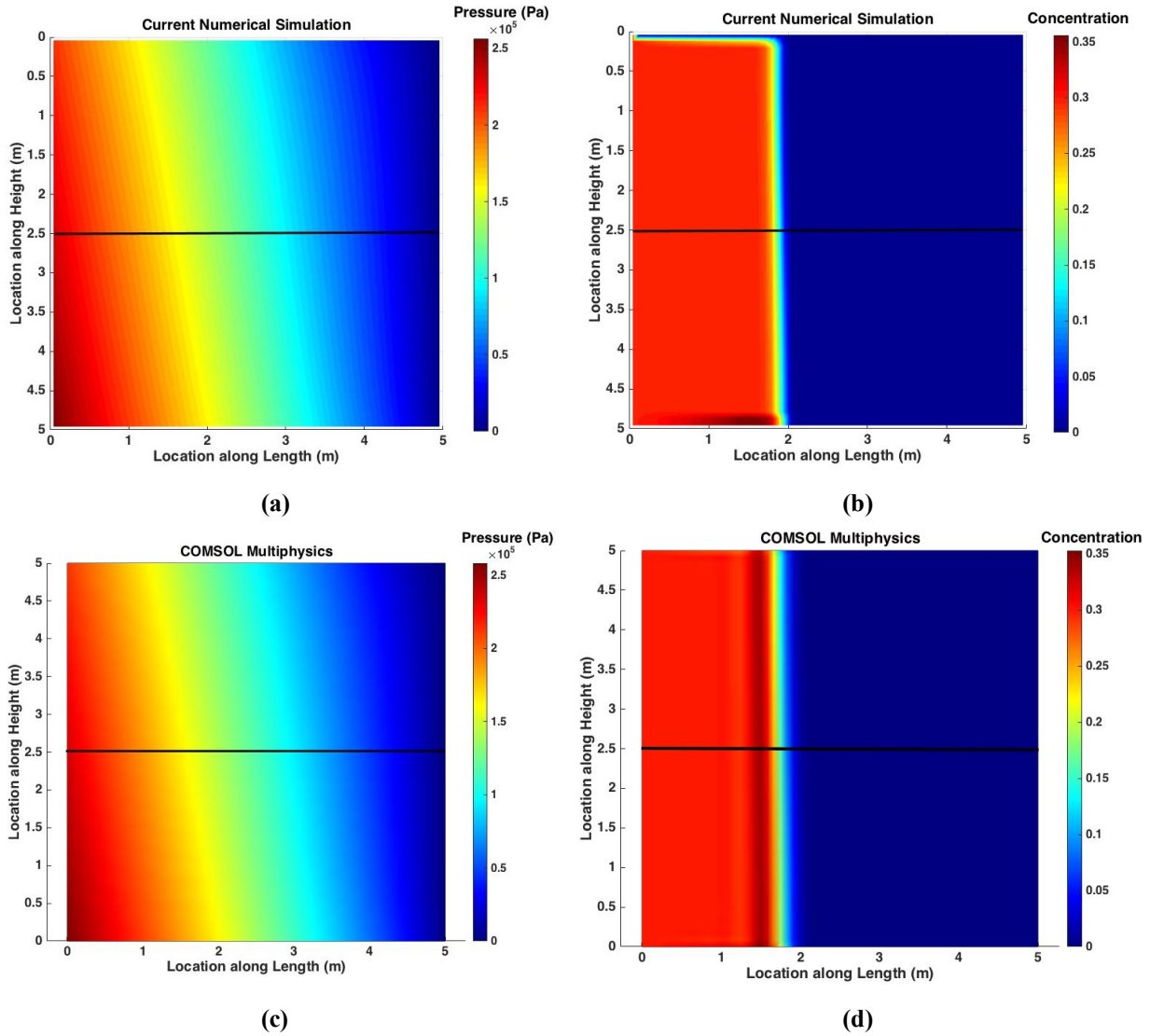
The model has been verified by comparison with the simulations conducted with COMSOL Multiphysics, which is a general purpose software platform, for modeling physics-based problems.

Figs. 4a and 4c compare the result of pressure field from COMSOL Multiphysics and our simulation when no proppant is injected at the left boundary. In this case, both COMSOL Multiphysics and our numerical simulator solve only Eq. 7 (slurry mass balance). Results indicate a general agreement between the predictions of the two models. In Fig. 4e, we compare the pressure profile along the cross section shown in Fig. 4a. The good match that is observed between these simulations results from the fact that traditional numerical schemes give accurate results when dealing with elliptic partial differential equations (Eq. 7).

Figs. 4b and 4d show the concentration contour plot after 20 seconds from the start of proppant injection for both the current computer code and COMSOL, respectively. Fig. 4f shows the concentration profile across the line shown in Fig. 4b.

A comparison between Figs. 4b and 4d indicates that the travel distances of proppant front for both simulations are the same at approximately 2 m from the left boundary. However, COMSOL simulation shows more numerical diffusion at the proppant front, while the results of our numerical technique indicate a sharper front and less numerical diffusion. According to Eq. 2, there is no second order space derivative in proppant transport equation. Even order derivatives indicate diffusion and, therefore, a suitable numerical technique in solving this type of problems is the one that results in minimum diffusion. According to Fig. 4f, COMSOL Multiphysics gives more gradual change in concentration gradient compared to our simulation. We can see how traditional numerical schemes fail close to shock fronts when dealing with hyperbolic partial differential equations.

The second difference is the oscillatory nature of the solution technique in COMSOL as can be seen in Fig. 4f. The oscillation originates from the fact that all traditional numerical techniques with orders higher than one generate oscillations in places with large gradients. This limitation does not exist in our numerical simulation as shown in Figs. 4d and 4e.



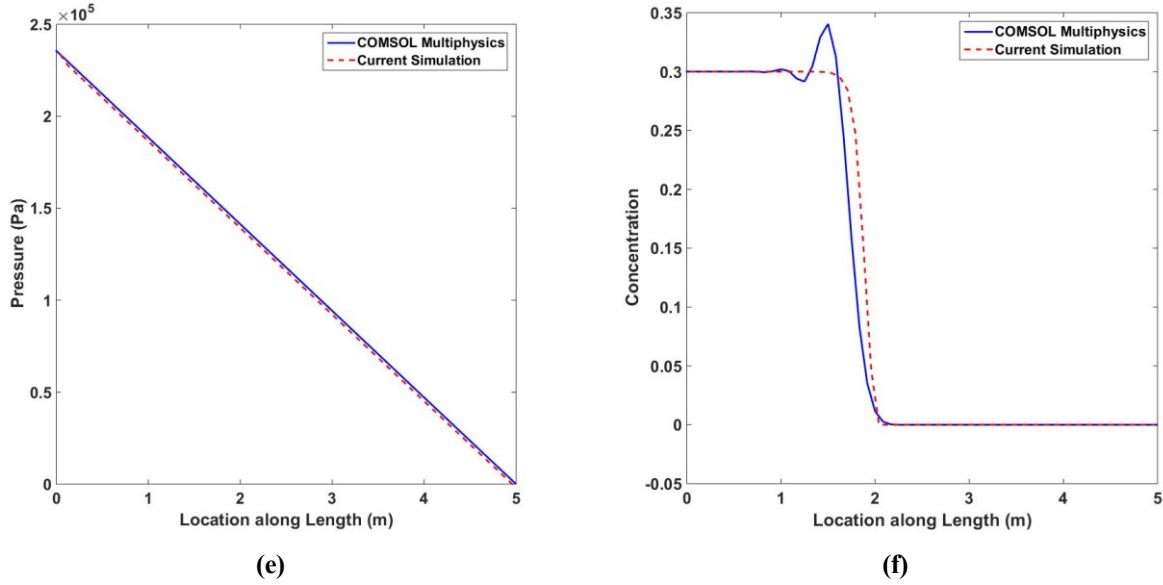


**Figure 4: Pressure and Concentration Distribution of COMSOL Multiphysics and presented model at 20 seconds**

### 6.3 Base Case Model

Table 1 shows the input parameters of the base case model. The simulation continued until the entire slot was filled with proppant.

**Table 1: Input parameters for the base model**

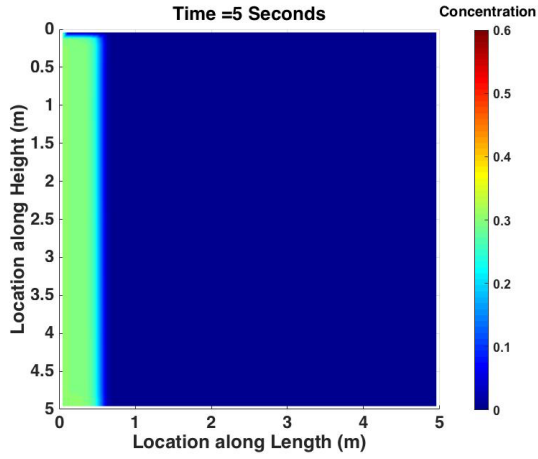
Fluid Flow Rate (lit/sec)	1.325
Proppant Diameter (mm)	0.200
Proppant Density ( $\text{kg/m}^3$ )	2,600
Fluid Viscosity (Pa sec)	0.4
Saturation Concentration*	0.6

\*This parameter was kept constant for all simulations.

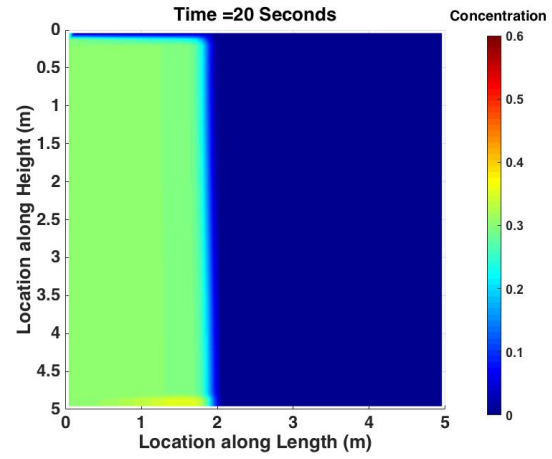
Fig. 5 shows the concentration maps at different times during the injection as predicted by the numerical transport model. The amount of particle concentration is indicated by the colour change in the contour plots. Figs. 5a and 5b show the proppant front continues to extend with no change in concentration as the slurry travels through the length of the model. The Buoyance number of the base case according to Eq. 44 is 3.00 and therefore, due to much higher proppant horizontal velocity relative to its vertical velocity in the specified condition of the simulation, little settlement is observed at the bottom of the slot before the proppant front reaches the right boundary. However, Figs. 5c-5f show a higher proppant concentration at the bottom of the slot, indicating the formation of a sediment bed.

A proppant bank is also created at the discharge part of the model when the front reaches the right boundary (Figs. 5e-5f). The bank grows with time in an unsymmetrical manner due to proppant

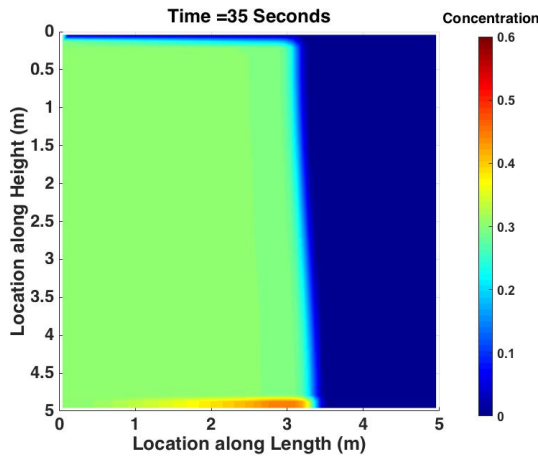
settlement. The proppant concentration increases to the saturation concentration after the proppant reaches the right boundary. We set the numerical proppant flux entering the element to zero when its proppant concentration reaches the saturation level.



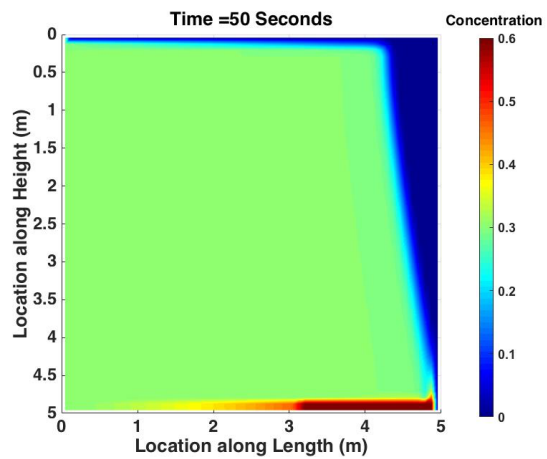
(a)



(b)



(c)



(d)

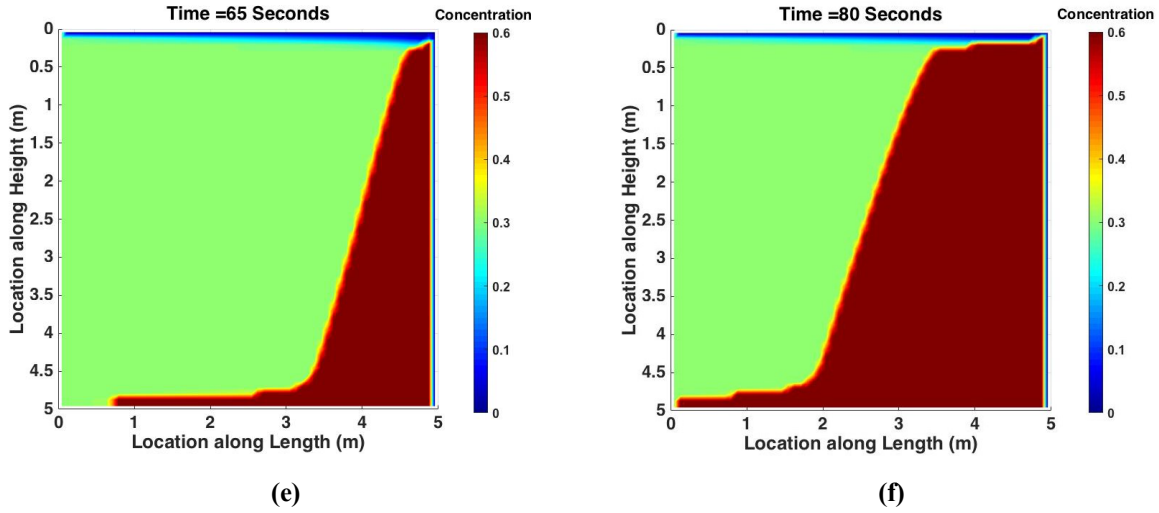
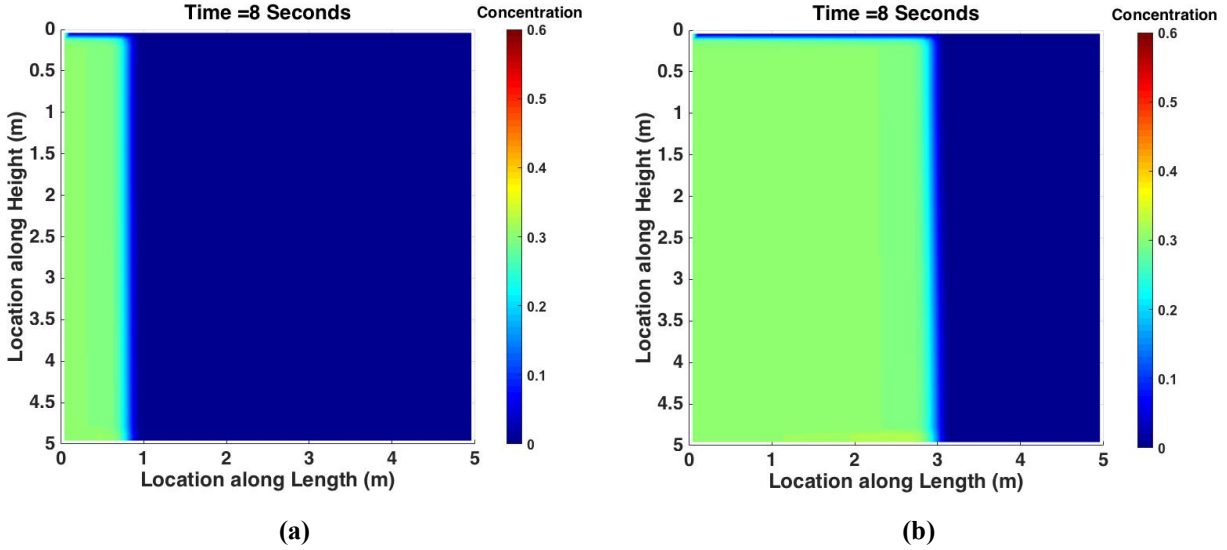
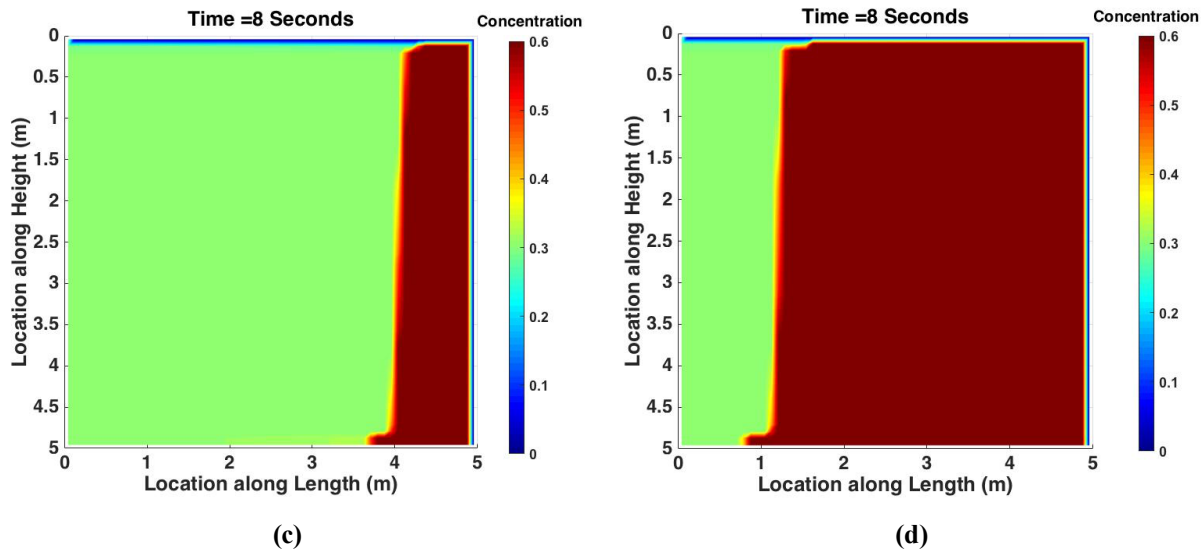


Figure 5: Concentration maps for the base model at different injection times

### 6.4 Effect of Volumetric Flow Rate

Fig. 6 shows proppant volume fraction contour plots at 8 seconds of injection for different volumetric injection rates of 1.3, 5.3, 10.6 and 15.9 lit/sec (720, 2,880, 5,760 and 8,640 bbl/day, respectively). The buoyancy number,  $N_{Bu}$  is increasing by increasing the flow rate. This means flow-rate increase favors horizontal flow. Buoyancy number for different volumetric injection rates of 1.3, 5.3, 10.6 and 15.9 lit/sec is 3, 12, 24, and 36 respectively. Obviously, the slot fills up faster at higher injection rates.





**Figure 6: Concentration map for injecting proppant with different volumetric flow rates of a) 1.325, b) 5.3, c) 10.6 and d) 15.9 lit/sec after 8 seconds**

Fig. 7 shows the time that is required for the proppant front to reach 4.5 m for different flow rates. Obviously, longer injection time is needed for the lower rates. For different volumetric injection rates of 1.3, 5.3, 10.6 and 15.9 lit/sec, this time is 46, 12, 6 and 4 seconds, respectively. The amount of settling is indicated by the creation of a higher concentration bed at the bottom of the slot, which is insignificant in all cases except for the lowest flow rate, as shown in Fig. 7a. This is mainly due to the fact that the horizontal proppant velocity for high-rate injections is one order of magnitude larger than vertical proppant velocity. If in some situations bed concentration reaches to saturation concentration, the created proppant bank alters the area available for fluid flow in the fracture and may cause a blockage at the fracture entrance and possibly lead to premature termination of the fracturing operation.

It should be noted that while the amount of settling is indicated by the size of the bed at the bottom of the fracture or the size of the region with clear fluid at the top of the fracture, the amount of convection can be recognized by the slope of the iso-concentration contours. The less this slope, the more the convection. Convection occurs because the heavier proppant slurry tend to fall to the bottom of the fracture and the low-viscosity particle-free fluid flows more easily at the top.

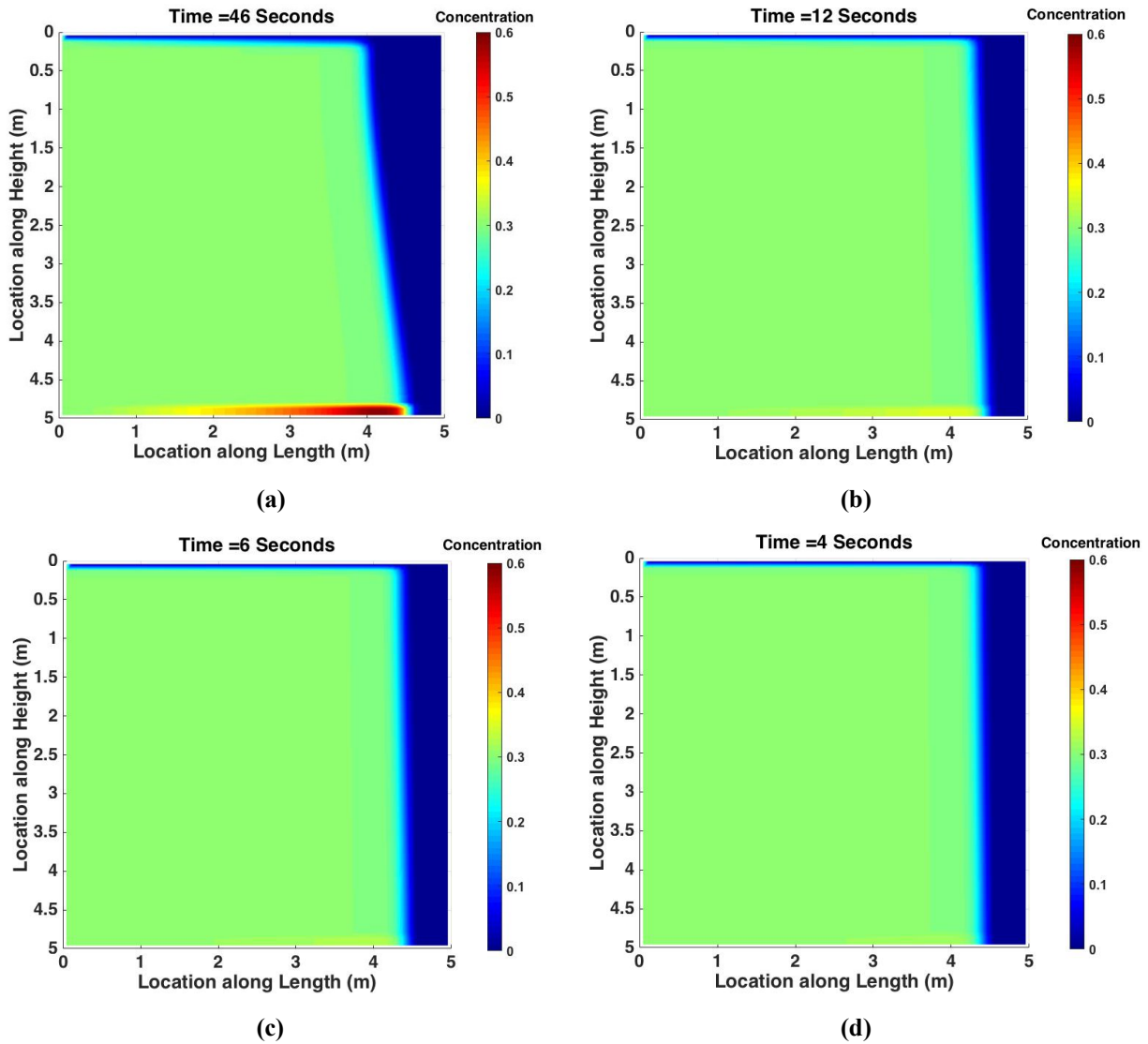
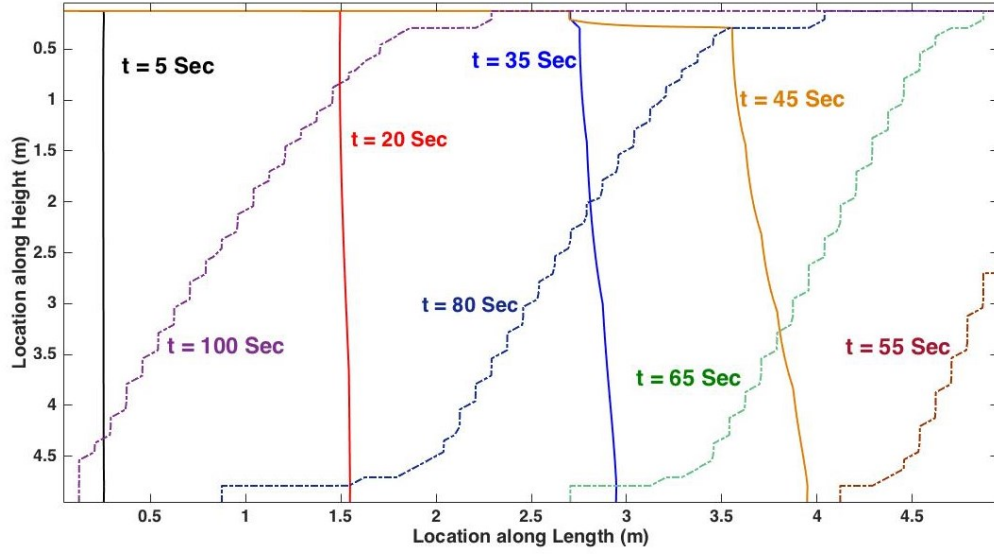
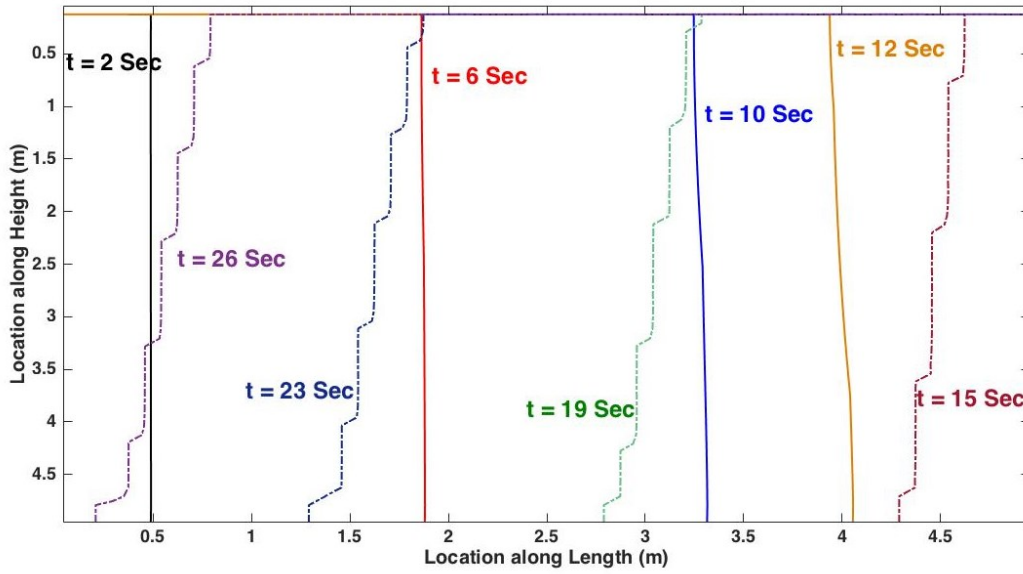


**Figure 7: Concentration map for injecting proppant with different volumetric flow rates of a) 1.3, b) 5.3, c) 10.6 and d) 15.9 lit/sec after a) 46, b) 12, c) 6 and d) 4 seconds**

Figs. 8a and 8b depict the proppant front, i.e. injection concentration of 0.3, for different flow rates during the injection. Solid lines show proppant front advancement before it reaches the right boundary of the model. Dashed lines show 0.6 concentration (saturation concentration front), which seems to be steeper for higher flow rates due to less convection flow at higher horizontal velocities. For the least flow rate case, a stronger convective transport is indicated by a smaller slope of the concentration contours. As expected, the slot is filled up faster for injection flow rates.

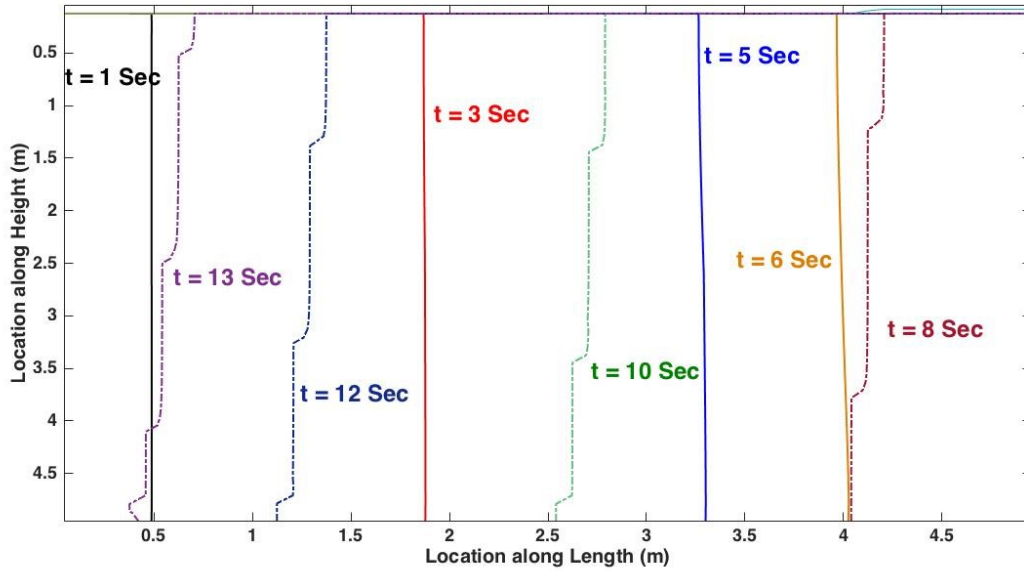


(a)  $q = 1.3$  lit/sec

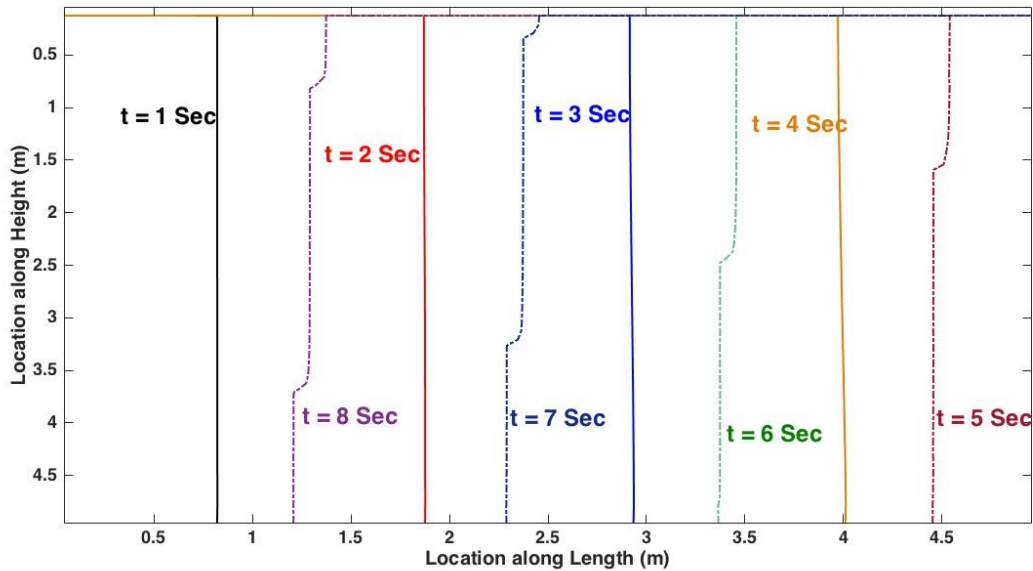


(b)  $q = 5.3$  lit/sec

Figure 8: Proppant fronts at different injection rates. Solid lines show the proppant front before reaching the right boundary of the model. Dashed lines show the proppant front after reaching the right boundary.



(a)  $q = 10.6$  lit/sec



(b)  $q = 15.9$  lit/sec

**Figure 9: Proppant fronts at different injection rates. Solid lines show the proppant front before reaching the right boundary of the model. Dashed lines show the proppant front after reaching the right boundary.**

In conclusion, it can be stated that flow rate has a strong impact on both settling and convection. Higher flow rate decreases settling and convection at the same time due to the fact that by increasing injection rate, viscous force overrides gravity force more and more. This in turn lead to proppant placement efficiency improvement. In the design applications, applying higher injection

rate can also create wider fracture and ease proppant entry. However, higher injection rate does not necessarily yield better proppant placement when height growth is expected. In this situation, a shorter propped length might be obtained.

### 6.5 Effect of Proppant Density

We applied four different proppant densities of 2100, 2600, 3100 and 3600 kg/m<sup>3</sup>. Fig. 10 shows the concentration contours at 40 seconds of injection. Clearly, settlement velocity increases for heavier proppants. As it is shown in the figures, a thin layer of proppant is formed at the bottom of the slot, before the front reaches the right boundary. For the selected input parameters in these simulations, changing the density of the proppant did not alter the proppant distribution significantly. This can be attributed to the relatively high viscosity of the injection fluid in these numerical exercises.

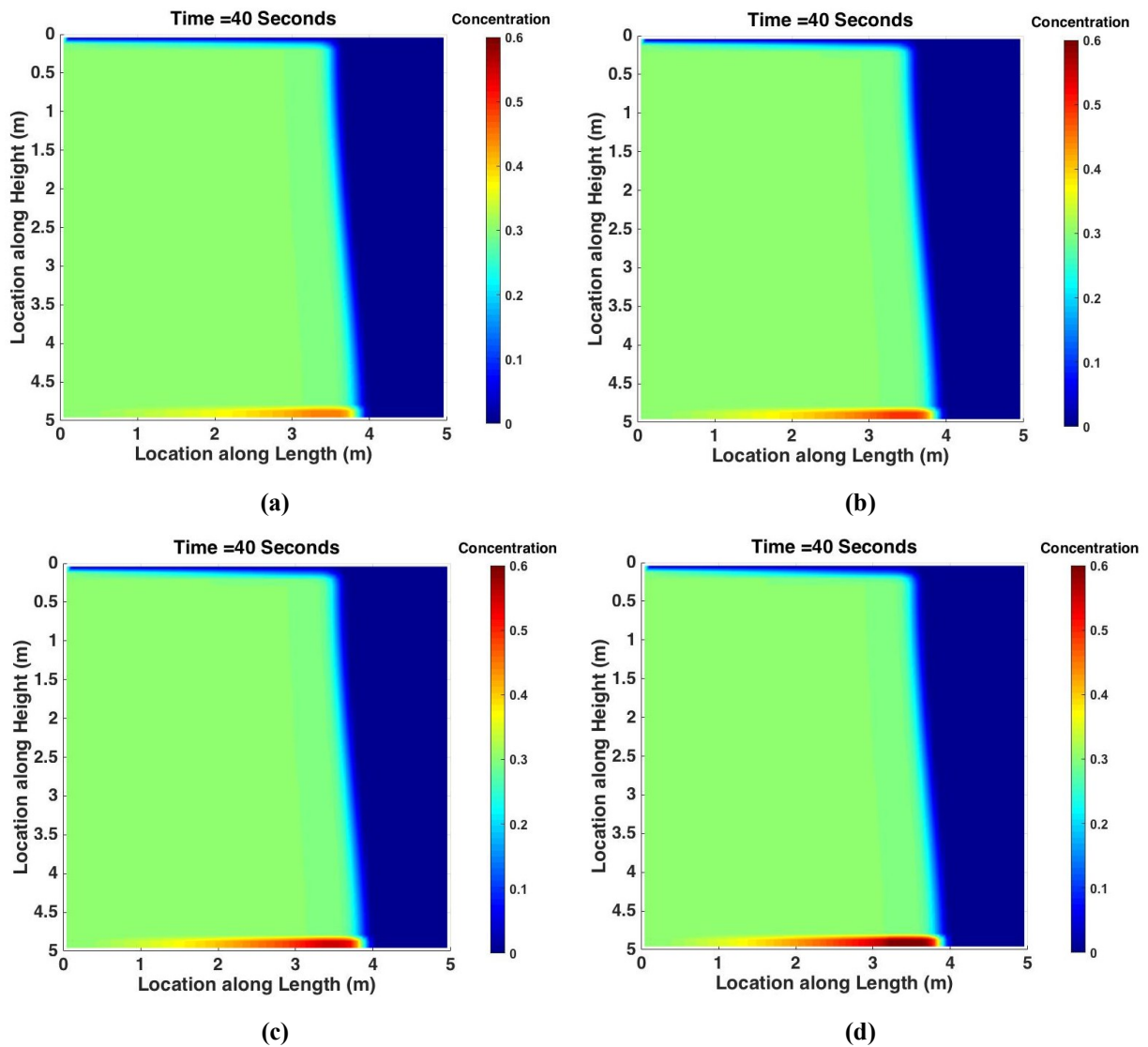


Figure 10: Concentration profile for different proppant densities of a) 2,100, b) 2,600, c) 3,100 and d) 3,600 kg/m<sup>3</sup> after 40 seconds of injection

## 6.6 Effect of Proppant Size

We applied different proppant diameters of 0.1, 0.6, 1.5 and 2.36 millimetres. These sizes are chosen based on the real proppant diameter range. It should be mentioned that in real case, the mobility of the proppants rapidly decreases when the fracture width is of the same order of magnitude as the proppant diameter. The fracture width should be 4 to 5 order of magnitude bigger than the particle density for effective placement. However, we have neglected this fact here since our focus is to observe the settling characteristics of the particles. This effect can be accounted for by simply imposing a minimum fracture width required for free proppant circulation, in the numerical code. Fig. 11 shows the proppant concentration profiles after 40 seconds of injection. Increasing proppant diameter has the same but stronger effect as increasing proppant density and causes more settlement by increasing the vertical velocity component of proppants. This is predictable since according to Eq. 38, proppant settling velocity is proportional to the square of the particle diameter, while it is only proportional to the density to the power of one.

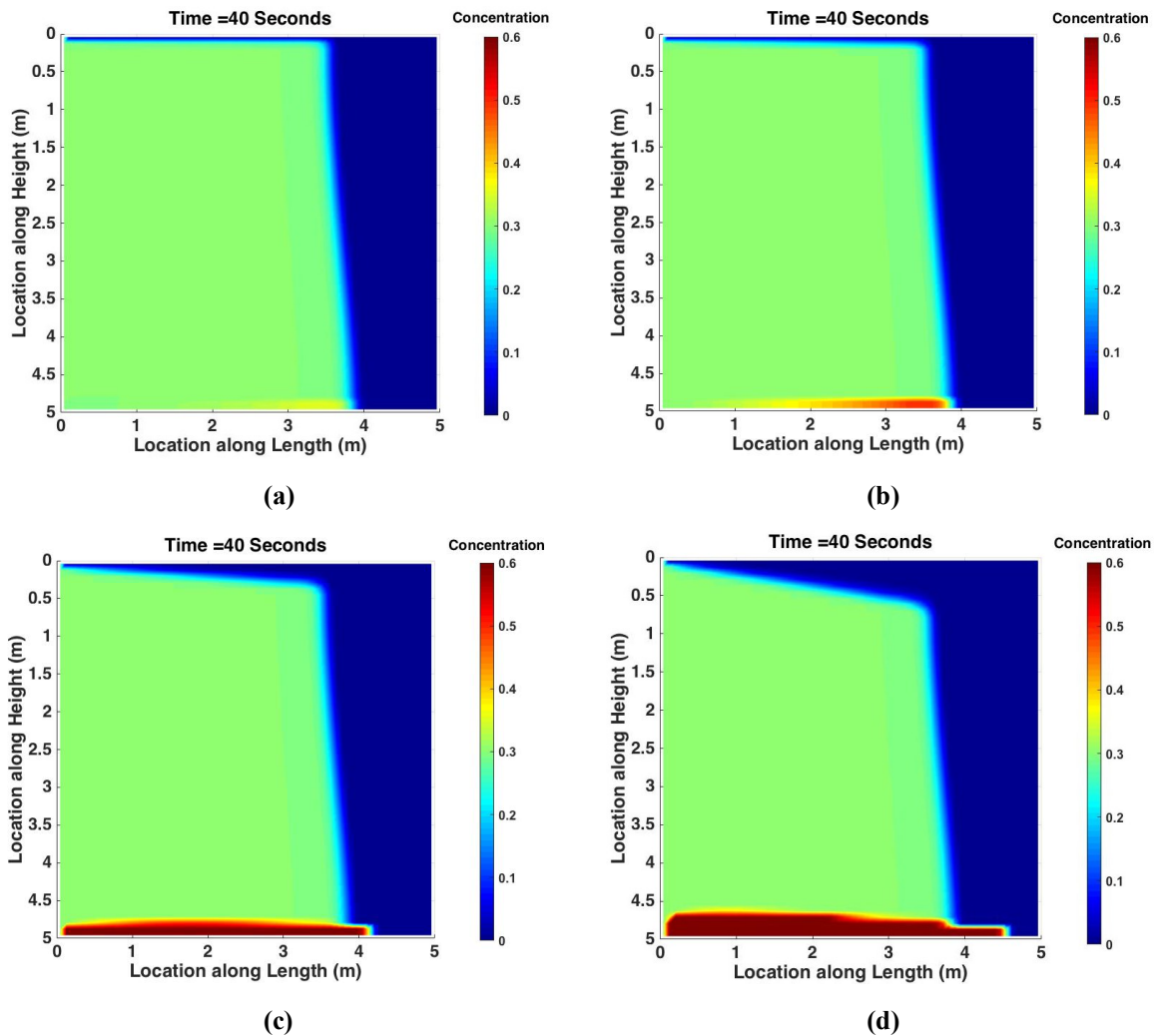


Figure 11: Concentration Maps for Different Proppant Diameters; a) 0.2 b) 1 and c) 2 mm, After 40 seconds of injection

## 6.7 Effect of Injection Fluid Viscosity

Figs. 12 and 13 show proppant volume fraction contour plots at 50 and 65 seconds of injection for four different fluid viscosities of 0.05, 0.1, 0.4 and 1 Pa Sec. For small values of viscosity, settlement is very strong, resulting in a buildup of particles at the bottom of the slot. It can be observed from these figures that at lower viscosities, concentration has reached the saturation value in a large portion of the slot height. This can cause premature termination of fracturing treatment since the carrying capacity of the injecting fluid reduces by reducing viscosity. Another issue with having low viscosity injection fluids is the creation of narrow fractures. If the width of the fracture is comparable to proppant diameter, the proppant transport can be altered significantly due to extra drag forces exerted on the proppants by the fracture walls.

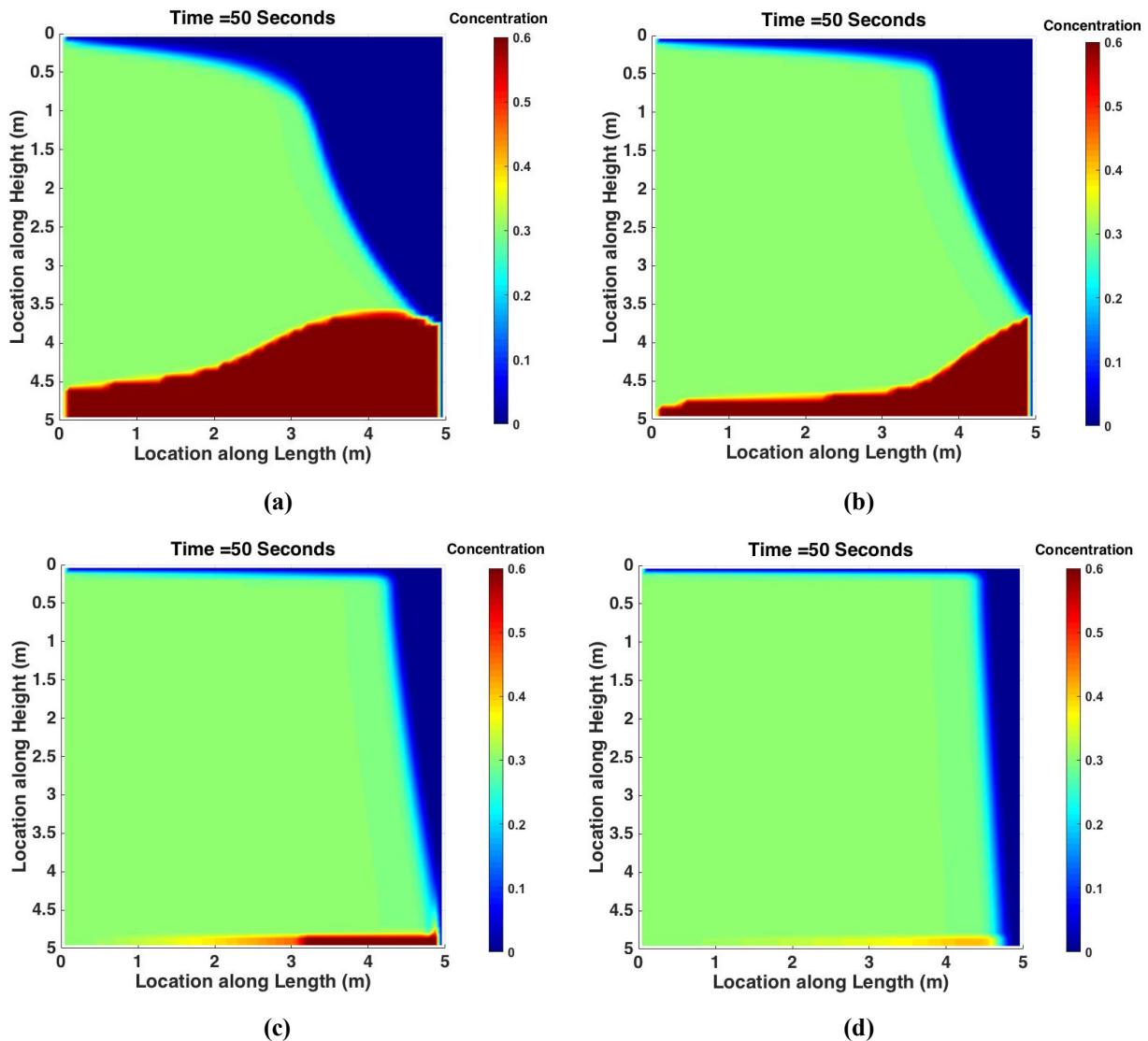
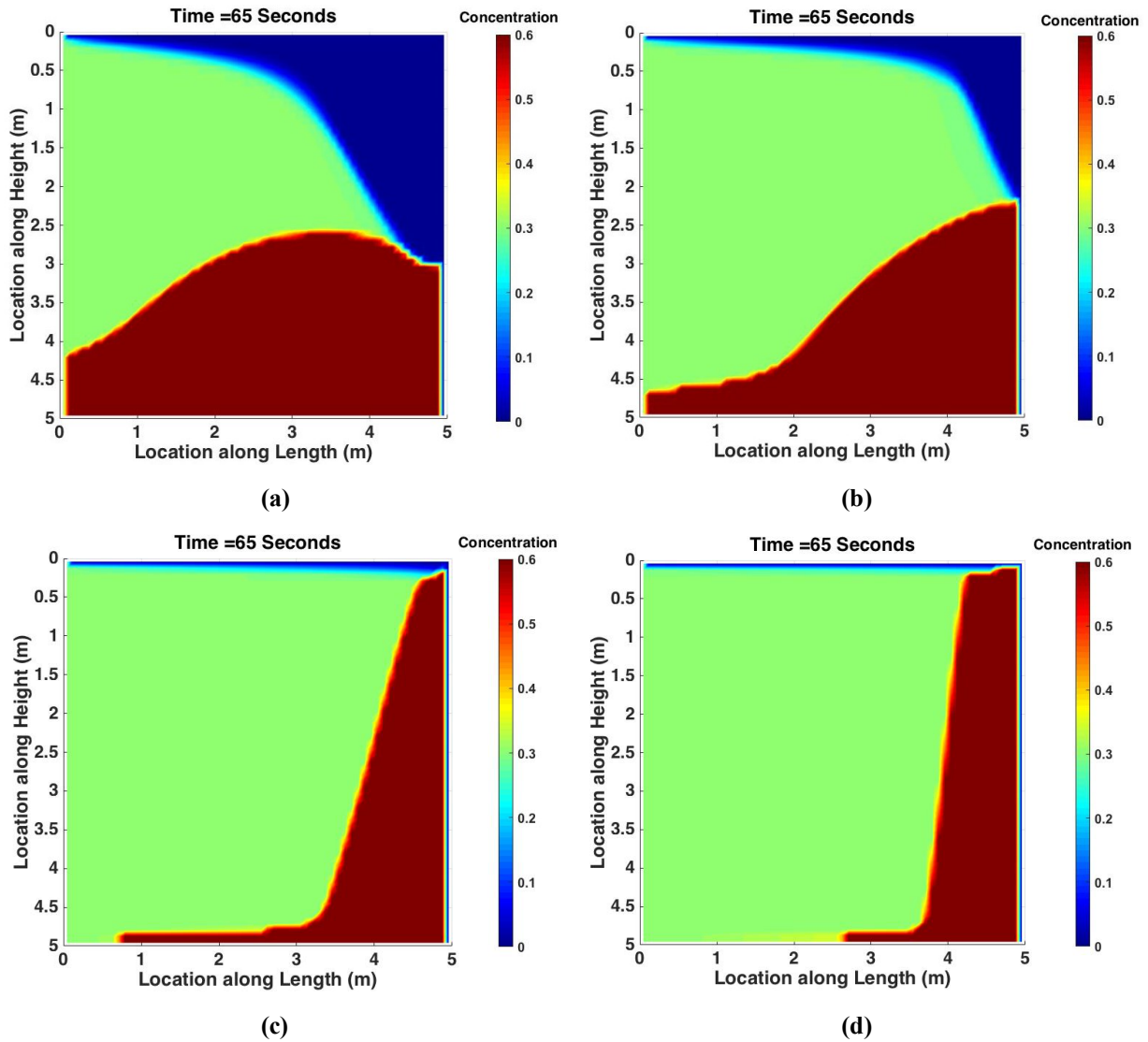


Figure 12: Concentration maps for different injection fluid viscosities; a) 0.01, b) 0.1, c) 0.4 and d) 1 Pa.Sec, after 50 seconds of injection



**Figure 13: Concentration maps for different injection fluid viscosities; a) 0.01, b) 0.1, c) 0.4 and d) 1 Pa.Sec, after 65 seconds of injection**

The Buoyancy number for the different simulated cases, as the viscosity increases are 0.375, 0.75, 3, and 7.5, displaying better carrying capacity for higher viscosity fluids. Based on the size of the bed at the bottom of the slot, settling is greatly enhanced in low viscosity fluids, while the slope of the concentration front in Fig. 13 shows convection is reduced in high viscosity fluids. Obviously, poor proppant placement should be expected specially when a long hydraulic fracture is created and a low viscosity fluid is used. Overall, viscosity is strongly effecting both settling and convection.

### 6.8 Elliptical Slot

The results presented so far related to the case of rectangular slot with uniform width of 3 mm along the entire fracture height. In this section, we change the width of the slot from rectangular

to elliptical to investigate the effect of fracture shape on proppant distribution. The width of the fracture here is calculated from:

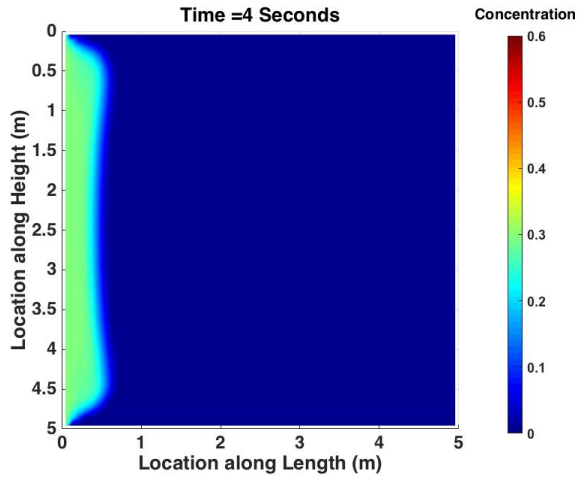
$$w = w_{centre} \left[ 1 - \left( \frac{2y}{h} \right)^2 \right]^{0.5} \quad (45)$$

where  $w_{centre}$  is the maximum width of the slot in the middle (5 mm),  $h$  is the height of the model (5 m), and  $y$  is the vertical axis with the coordinate origin placed at the middle of the fracture.

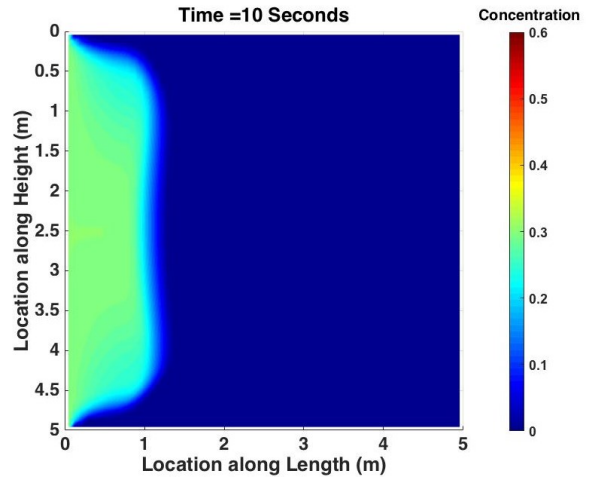
Fig. 14 shows the concentration map for the elliptic slot at different injection times. It is interesting that the concentration distribution is greatly different compared to the rectangular case. The reason is that for elliptical slots, horizontal slurry velocity is calculated from Eq. 46 (Nordgren, 1972) instead of Eq. 5:

$$u_{sl} = - \frac{\pi w^2}{64\mu} \frac{\partial p}{\partial x} \quad (46)$$

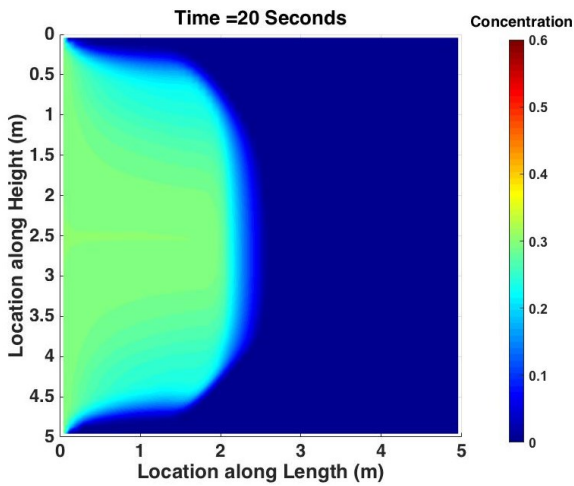
Obviously, proppant particles travel faster in the middle part of the slot, where the width is the greatest and offers least resistance to flow. In addition, at the top and bottom of the model the width is less than particle diameter. Therefore, both top and bottom of the slot are not covered by proppants. In real situations where there is leak off of injection fluid to formation, proppant will have some tendency to move towards the edges of the fracture. Therefore, leakoff reduces the tendency for proppant packing in the center part of the elliptic fracture to some extent.



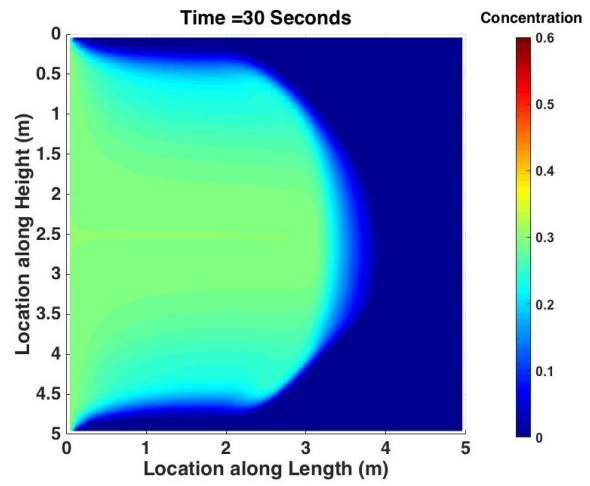
(a)



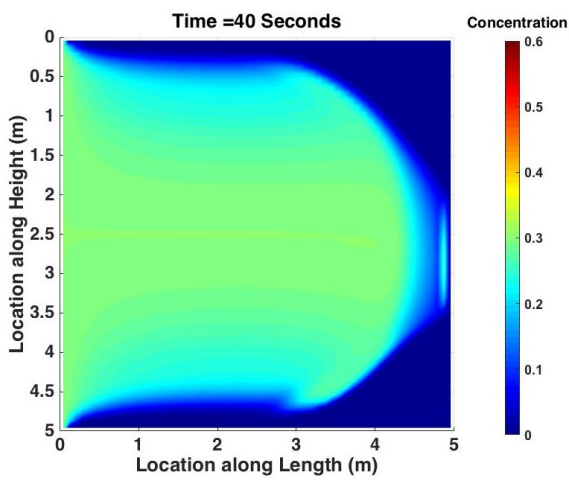
(b)



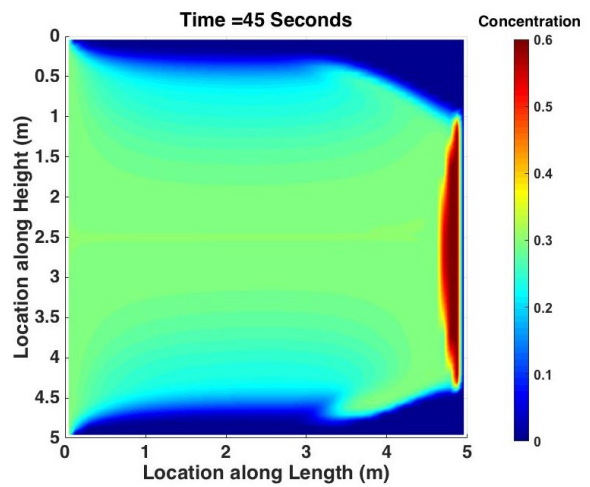
(c)



(d)



(e)



(f)

Figure 14: Simulation Result of Presented Model for Elliptic Slot

## 6.9 Buoyancy Number

As the proppants are injected inside the fracture, the density of the carrying fluid starts to increase, generating a density gradient along the fracture. This density gradient, even in its moderate amount, can generate large-scale fluid movement which dominates the particle settling in most field scale conditions. This complex phenomenon causes vertical segregation of suspensions of different density.

To confirm the effectiveness of Buoyancy number in predicting dominance of gravity over viscous forces, several simulation examples were carried out and the results are presented in this section. In the previous simulations, it was evident that as the Buoyancy number was increased, the downward flow tendency of the slurry to the bottom of the slot decreased and a more symmetrical proppant distribution were obtained. To better verify this, two simulations were conducted in which Buoyancy number was set to 0.1 and 1. Fig. 15 shows the concentration distribution for abovementioned Buoyancy number at times that the front has advanced 2 m. As shown in Fig. 15, the lower slope of the concentration front indicates higher convection. At the same time, higher convection means more lateral advancement of concentration front at the bottom of the fracture. Even at Buoyancy number of 1 the tendency of the injected slurry to go to the bottom of the slot is not diminished. Simulations at higher Buoyancy number results in an increase in the symmetry of the concentration distribution. That is because a more uniform flow into the slot is expected when  $N_{Bu}$  is higher.

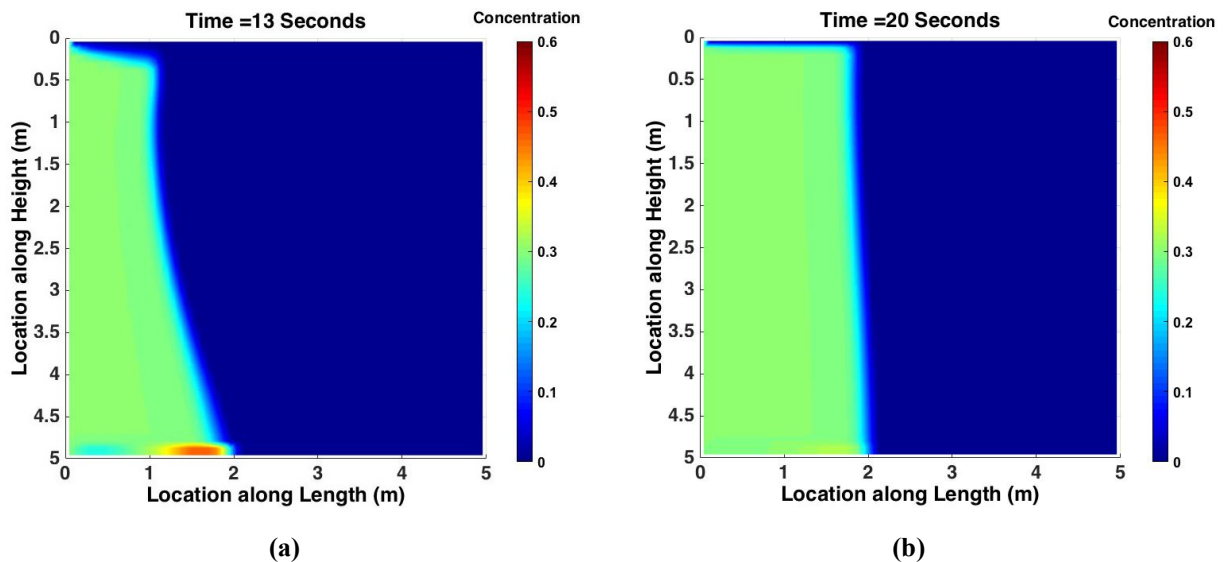
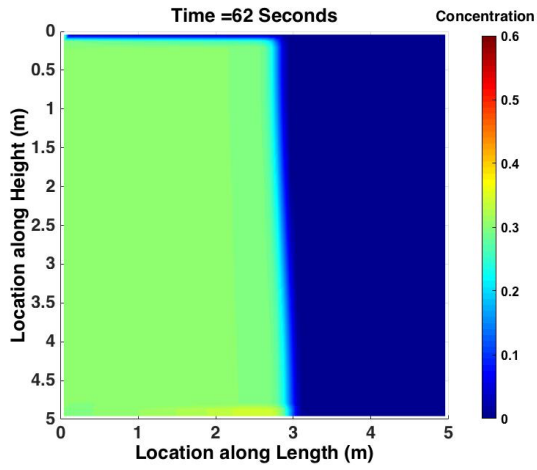
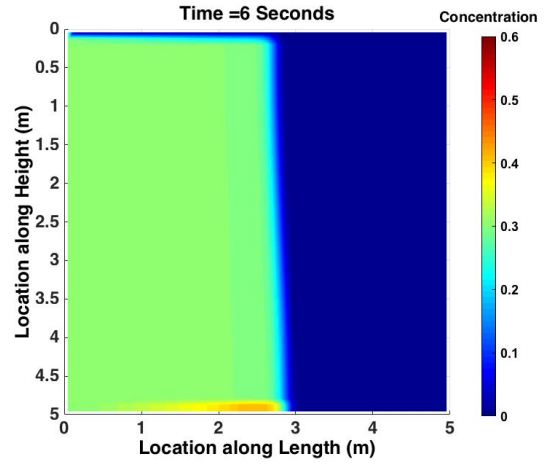


Figure 15: Effect of Buoyancy number on Convective Flow: a)  $N_{Bu}=0.1$ , b)  $N_{Bu}=1$

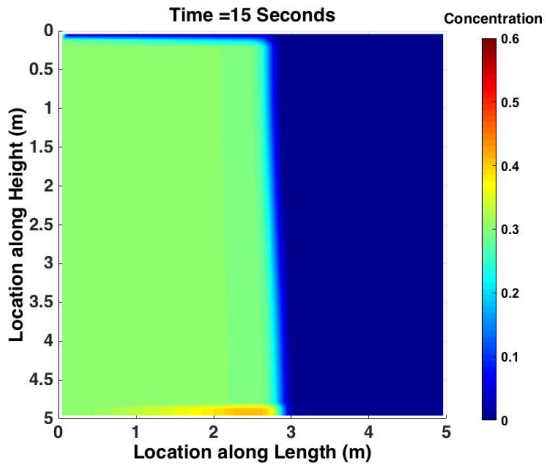
It is interesting to note that the shape of concentration front depends only upon the value of Buoyancy number and not on a particular input parameter. In a series of simulations, two parameters from equation 4.7 were changed in a way that the value of Buoyancy number was kept constant. Fig. 16 shows the simulation results when concentration front has reached 3 m of the model domain and density-width, flow rate-density, flow rate-viscosity, flow rate-width, density-viscosity and width-viscosity are changed in each case.



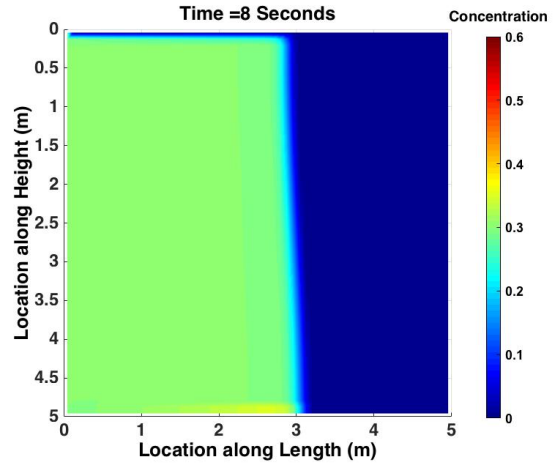
a)  $w=0.003 \times 2$  m,  $\Delta\rho=1600/8$  kg/m<sup>3</sup>



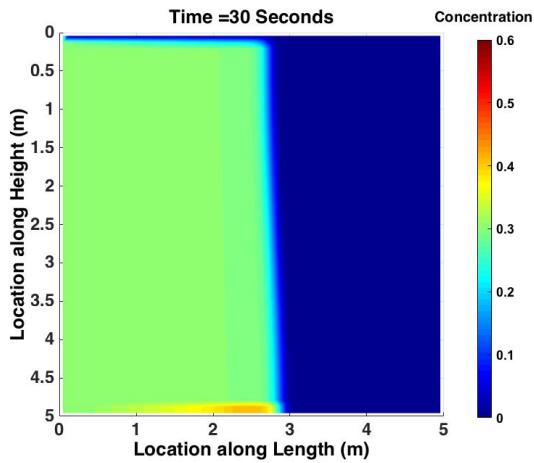
b)  $q=0.003 \times 5$  m<sup>3</sup>/s,  $\Delta\rho=1600 \times 5$  kg/m<sup>3</sup>



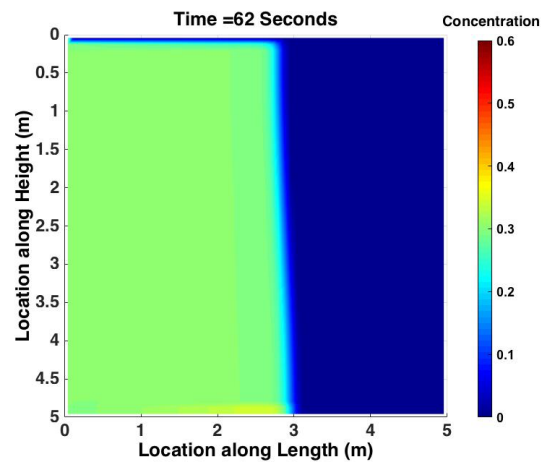
c)  $q=0.003 \times 2$  m<sup>3</sup>/s,  $\mu=0.4/2$  Pa.s



d)  $q=0.003 \times 8$  m<sup>3</sup>/s,  $w=0.003 \times 2$  m



e)  $\mu=0.4 \times 5$  Pa.s,  $\Delta\rho=1600 \times 5$  kg/m<sup>3</sup>



f)  $\mu=0.4 \times 8$  Pa.s,  $w=0.003 \times 2$  m

Figure 16: Constant Buoyancy Number and Similarity of Concentration Plume

The general shape of all the concentration fronts are the same. The size of the concentration plume might vary a bit since it is difficult to capture the time at which identical sizes are obtained. The amount of settling is different in some cases and that is due to the fact that Buoyancy number is not a measure of the settling. In addition, since the velocity field is different for different simulations, the time at which concentration front reaches a certain point is also different.

In real placement designs, it is assumed that proppants are uniformly distributed inside the fracture. However, strong gravity driven motions can cause this distribution uniformity to be lost over the total or part of the fracture height. Production from the upper section of the payzone can be dramatically reduced if proppants did not extend vertically through the fracture height and instead misplaced at the bottom of the fracture.

## **7. Discussion of Results**

During proppant injection, vertical motion of the proppants affects the final distribution and can lead to creation of a proppant bed at the bottom of the fracture. The concentration of proppants inside the bank can reach its maximum value which is the saturation concentration. If the bank covers a major portion of the fracture height, it can block further proppant injection leading to premature termination of the proppant injection. The amount of vertical motion of proppants depends on the volumetric injection rate, suspending fluid viscosity, proppant density and proppant size. Overall, these parameters impact the concentration distribution by changing proppant velocity fields. Low suspending fluid viscosity, high proppant density, large proppant sizes and low injection rate can enhance the proppant settlement.

According to our simulations, the viscosity of the carrying fluid is the most important parameter in controlling lateral transport dominance over settling. Among other factors, density of the particles has a small impact on the final distribution of the proppants.

Based on the proppant distribution for elliptic slots, we can conclude that fracture shape can affect slurry convection and settlement. Convection was stronger than settlement in the cases we attempted since no bed was created in our simulations.

In field-scale fracture designs, the fluid velocity will be affected by several other variables such as fluid leak off, non-uniform proppant size distribution or non-spherical particles. Although we neglected these factors, our modelling results can still be used to improve treatment designs. For example, we can obtain an estimate of the flow rate which will disperse proppants more uniformly over the fracture height, without creating a bed at the bottom. Similarly, a low pump rate in the order of leak off rate will confine the particles at the bottom of the fracture rendering an ineffective frac-packing operation.

## **8. Conclusion**

We have numerically simulated proppant transport inside slots by solving equations of motion of slurry and proppants. We assumed incompressible and Newtonian fluid and an isothermal system. We accounted for the change of the viscosity of the slurry due to the change of proppant concentration. An effective numerical technique was used to capture the proppant front more precisely and with minimum oscillation and diffusion. In this numerical scheme, WENO scheme of finite volume was employed to approximate the solution of the hyperbolic transport partial

differential equation. We used dimensional splitting technique to reduce the running time and complexity of solving hyperbolic partial differential equations.

We investigated the effects of injection rate, proppant density, proppant size and injection fluid viscosity on proppant placement. These parameters change the final proppant concentration distribution since they control particle settlements. Some of the conclusions from the sensitivity analysis presented in this paper include:

- The model simulated proppant bank creation at the bottom of the fracture during the treatment time.
- The fracture fills up faster at higher injection rates with less proppant settlement.
- Viscosity of the carrying fluid has the strongest effect on the amount of proppant settlement.
- Within practical ranges, parameters such as proppant size and density only have a modest effect on proppant settlement.

As of now, there is a significant uncertainty in the effect of physical proppant and fluid parameters on the final proppant distribution. The numerical model presented here enhances our understanding of the relationship between fluid and proppant properties and the final proppant distribution that determines the conductivity of the propped fracture. The outcome is improved design and implementation of the fracpack operation and reduced uncertainty in the fracpack performance.

### **Acknowledgment**

The authors would like to acknowledge the research funding for this study provided by NSERC through CRDPJ 387606-09.

### **Nomenclature**

$c$	Volumetric Concentration of Proppants
$c^*$	Saturation Concentration
$d_p$	Proppant Diameter
$f(c)$	Concentration Factor
$f(w)$	Wall Factor
$\hat{f}$	Numerical Flux Function
$g$	Acceleration due to Gravity
$h$	Height of the Model
$N_{Bu}$	Buoyancy Number
$p$	Pressure
$Q_h$	Horizontal Flow rate

$q_{inj}$	=	Injection Flow Rate
$t$	=	Time
$u$	=	Horizontal Velocity
$u_f$	=	Fluid Horizontal Velocity
$u_p$	=	Proppant Horizontal Velocity
$u_{sl}$	=	Slurry Horizontal Velocity
$v$	=	Vertical Velocity
$v_f$	=	Fluid Vertical Velocity
$v_{inertia}$	=	Corrected Settling Velocity of Proppants for Inertia
$v_p$	=	Proppant Vertical Velocity
$v_{sl}$	=	Slurry Vertical Velocity
$v_{set}$	=	Settling Velocity
$v_t$	=	Terminal Velocity
$w$	=	Fracture Width
$w_{centre}$	=	Maximum Width of elliptic slot
$x$	=	Horizontal Coordinate
$y$	=	Vertical Coordinate
$\Delta x$		Gridcells Size
$\mu$	=	Viscosity
$\mu_0$	=	Initial Viscosity
$\mu_{sl}$	=	Slurry Viscosity
$\rho$	=	Density
$\rho_p$	=	Proppant Density
$\rho_f$	=	Fluid Density
$\rho_{sl}$	=	Slurry Density

## 9. References

- Adachi, J., Siebrits, E., Peirce, A., & Desroches, J. (2007). Computer simulation of hydraulic fractures. *International Journal of Rock Mechanics and Mining Sciences* , 44 (5), 739–757.
- Allen, H. S. (1900). L. The motion of a sphere in a viscous fluid. *The London, Edinburgh, and Dublin Philosophical Magazine and Journal of Science*, 50(306), 519-534.
- Al-quraishi, A. A., & Christiansen, R. L. (20-23 February, 1999). Dimensionless Groups for Interpreting Proppant Transport in Hydraulic Fractures. Middle East Oil Show and Conference. Bahrain: Society of Petroleum Engineers.
- Barree, R., & Conway, M. (1994). Experimental and Numerical Modeling of Convective Proppant Transport. SPE Annual Technical Conference and Exhibition, 25-28 September, New Orleans, Louisiana. Society of Petroleum Engineers.
- Barree, R., & Conway, M. (1995). Experimental and Numerical Modeling of Convective Proppant Transport (includes associated papers 31036 and 31068 ). *Journal of Petroleum Technology*, 47 (03), 216 - 222.
- Batchelor, G. K. (1972). Sedimentation in a dilute dispersion of spheres. *Journal of Fluid Mechanics*,52(02), 245. doi:10.1017/s0022112072001399
- Bayo Shokir, E. E.-M., & Al-Quraishi , A. A. (15-18 April, 2007). Experimental and Numerical Investigation of Proppant Placement in Hydraulic Fractures. Latin American & Caribbean Petroleum Engineering Conference. Buenos Aires, Argentina: Society of Petroleum Engineers.
- Behr, A., Mtchedlishvili, G., Friedel, T., & Haefner, F. (2006). Consideration of Damaged Zone in a Tight Gas Reservoir Model With a Hydraulically Fractured Well. *SPE Production & Operations* , 21 (02), 206 - 211.
- Bird, R., Stewart, W., and Lightfoot, E. (1976). *Transport Phenomena*. John Wiley and sons.
- Clark, P., & Quadir, J. (1981). Prop Transport In Hydraulic Fractures: A Critical Review Of Particle Settling Velocity Equations. SPE/DOE Low Permeability Gas Reservoirs Symposium, 27-29 May, Denver, Colorado. Society of Petroleum Engineers.
- Clift, R. (1978). *Bubbles. Drops and Particles*.
- Daneshy, A. A. (1978). Numerical Solution of Sand Transport in Hydraulic Fracturing. *Journal of Petroleum Technology* , 30 (01), 132-140.

- Du, M. C., Zhan, L., Li, J., Zhang, X., Church, S., Tushingham, K., et al. (30 October-2 November, 2011). Generalization of Dual-Porosity-System Representation and Reservoir Simulation of Hydraulic Fracturing-Stimulated Shale Gas Reservoirs. SPE Annual Technical Conference and Exhibition. Denver, Colorado, USA: Society of Petroleum Engineers.
- Economides, M. J., & Nolte, K. (2000). Reservoir Stimulation. Sugar Land, Texas: John Wiley and Sons Ltd.
- Eskin, D., & Miller, M. J. (2008). A model of non-Newtonian slurry flow in a fracture. Powder Technology, 182 (2), 313–322.
- Frieauf, K. (2009). Simulation and Design of Energized Hydraulic Fractures. University of Texas at Austin, Ph.D. Thesis.
- Gadde, P., Yajun, L., Norman, J., Bonnecaze, R., & Sharma, M. (2004). Modeling Proppant Settling in Water-Fracs. SPE Annual Technical Conference and Exhibition, 26-29 September, Houston, Texas. Society of Petroleum Engineers.
- Govier, G. W., & Aziz, K. (1972). The Flow of Complex Mixtures in Pipes. Van Nostrand Reinhold Co.
- Hammond, P. S. (1995). Settling and Slumping in a Newtonian Slurry, and Implications for Proppant Placement During Hydraulic Fracturing of Gas Wells. Chemical Engineering Science, 50, 3247-3260.
- Horri, B. A., Ranganathan, P., Selomulya, C., & Wang, H. (2011). A new empirical viscosity model for ceramic suspensions. Chemical Engineering Science, 66(12), 2798-2806. doi:10.1016/j.ces.2011.03.040
- Koos, E. (2009). Rheological measurements in liquid-solid flows (Doctoral dissertation, California Institute of Technology).
- Lavrov, A. (2011). Models for Proppant Transport and Deposition in Hydraulic Fracture Simulation, A Review of the State of the Art. Trondheim, Norway: SINTEF Petroleum Research.
- Leveque, R. J. (2004). Finite Volume Methods for Hyperbolic Problems. Cambridge: Cambridge University Press.
- Liu, Y. (2006). Settling and Hydrodynamic Retardation of Proppants in Hydraulic Fractures. University of Texas at Austin, Ph.D. Thesis.
- Miranda, C. G., Soliman, M., Settari, A., & Krampol, R. (2010). Linking Reservoir Simulators with Fracture Simulators. SPE Eastern Regional Meeting, 13-15 October, Morgantown, West Virginia, USA. Society of Petroleum Engineers.

- Mobbs, A. T., & Hammond, P. S. (2001). Computer Simulations of Proppant Transport in a Hydraulic Fracture. *SPE Production & Facilities* , 16 (02), 112-121.
- Nordgren, R. (1972). Propagation of a Vertical Hydraulic Fracture. *Society of Petroleum Engineers Journal*, 12(04), 306 - 314.
- Novotny, E. J. (1977). Proppant Transport. SPE Annual Fall Technical Conference and Exhibition, 9-12 October, Denver, Colorado. Society of Petroleum Engineers.
- Ouyang, S. (1994). Propagation of Hydraulically Induced Fractures with Proppant Transport. University of Texas at Austin. Ph.D. Dissertation.
- Pearson, J. (1994). On suspension transport in a fracture: framework for a global model. *Journal of Non-Newtonian Fluid Mechanics*, 54, 503-513.
- Prandtl, L., & Tietjens, O. (1931). *Hydro-und Aeromechanik: nach Vorlesungen von L. Prandtl*. J. Springer.
- Ribeiro, L. H. (2013). Development of a Three-Dimensional Compositional Hydraulic Fracturing Simulator for Energized Fluids. The University of Texas at Austin.
- Schiller, L. (1932). Fallversuche mit Kugeln und Scheiben. *Handbuch der Experimentalphysik*, 4, 339-398.
- Settari, A., & Puchyr, P. (1990). Partially Decoupled Modeling of Hydraulic Fracturing Processes. *SPE Production Engineering* , 5 (1), 37 - 44.
- Shaoul, J., Behr, A., & Mtchedlishvili, G. (2007). Developing a Tool for 3D Reservoir Simulation of Hydraulically Fractured Wells. *SPE Reservoir Evaluation & Engineering* , 10 (01), 50-59.
- Sharma, M. M., & Gadde, P. B. (2005). The Impact of Proppant Retardation on Propped Fracture Length. SPE Annual Technical Conference and Exhibition, 9-12 October, Dallas, Texas. Society of Petroleum Engineers.
- Stokes, G. (1850). On the Effect of the Internal Friction of Fluids on the Motion of Pendulums. *Cambridge Philosophical Society*, 9(02), 8-106.
- Unwin, A. T., & Hammond, P. S. (8-10 March, 1995). Computer Simulations of Proppant Transport in a Hydraulic Fracture. SPE Western Regional Meeting. Bakersfield, California: Society of Petroleum Engineers.
- Wieselsberger, C. (1922). Further information on the laws of fluid resistance.

